Journal of Mechanical Engineering Research and Developments
ISSN: 1024-1752
CODEN: JERDFO
Vol. 45, No. 2, pp. 123-150
Published Year 2022

Impact of Cavity Location on Base Pressure at Supersonic Mach 1.8

Ridwan, Nur Husnina Muhamad Zuraidi, and Sher Afghan Khan*

Department of Mechanical and Aerospace Engineering, Faculty of Engineering, International Islamic University Malaysia, 50728 Kuala Lumpur, Malaysia.

*Corrosponding Author Email: sakhan@iium.edu.my

ABSTRACT

In this day and age, researchers and engineers are actively exploring research in the supersonic Mach number flow field, primarily related to the base pressure of aerospace vehicles and nozzle variants. The boundary layer theory explained the flow separation caused by fluid motion. The turbulent boundary layer at the base will generate supersonic expansion flow in the recirculation zone, resulting in a pressure decrease at the base region and a free viscous layer from the base region towards the free stream direction. Several experimental studies on base pressure and flow development have been conducted with sudden expansion. Base pressure is affected by the geometry of the passage, the area ratio, and the L/D ratio. Numerical simulation simulates the flow from a Converging-Diverging nozzle that has suddenly expanded into an enlarged duct with a cavity. The Mach number for this study is 1.8, and the area ratio is 2.56. The L/D ratio considered was from 1 to 10. The nozzle pressure ratio and aspect ratio of the cavity were considered in this study. The study investigates the impact of cavity location from the base wall toward the base pressure using Computational Fluid Dynamics. The simulated nozzle pressure ratio was for over, under, and ideally expanded cases. The results show that the NPR and cavity location from the base wall strongly influenced the base pressure.

KEYWORDS

base pressure; passive control; Computational Fluid Dynamics (CFD)

INTRODUCTION

The shear layer divides baseflow into two central regions. The shear layer will generate strong vortices, increasing the overall drag force, and the net drag force is made up of skin friction, wave, and base drag. There are two primary techniques for reducing base drag. As a result, base pressure influences base drag. These two base variables are inversely proportional to each other, so as base pressure rises, base drag falls, and vice versa. Also, as base drag decreases, the range of aerodynamic devices expands. The flow control method used is a cavity. The passive control technique is the primary focus. The purpose of flow control is to disrupt the base flow. The Cavity geometry is used to manipulate the flow. As a result, the base pressure will rise while the base drag will fall. The passive control technique in a cavity is the primary focus. The purpose of the cavities is to raise the base pressure. The effect of cavities as a passive controller on base pressure at supersonic Mach number was investigated in this study.

There is a distinction in drag form between the subsonic and supersonic flow. The drag in subsonic flow comprises skin friction drag and base drag, whereas wave drag is added in supersonic flow. First, skin friction drag is produced due to viscosity, accelerating this boundary layer air in the direction of travel [1]. Because skin friction drag is a solid-fluid interaction, the drag depends on both the solid and fluid properties. Finally, rough surfaces will have higher skin friction than smooth surfaces. Second, base drag is caused by negative pressure behind a projectile's base. The influence of the upstream boundary layer keeps it going. Third, wave drag refers to the drag caused by the formation of shocks at supersonic and high supersonic speeds [1]. When an aircraft reaches the speed of sound, shock waves are created along the surface. The shock waves change the static pressure and cause total pressure loss. Wave drag is related to the development of shock waves. The magnitude of wave drag is proportional to the flow's Mach number. As a result, shock waves are nothing more than an air disruption caused by high airflow speeds.

The condition of the forced flow of the fluid can be used to calculate the fluid flow. External flow is defined as the flow of an unbounded fluid over a surface. Second, internal flow refers to flow in a pipe that is entirely bounded by solid surfaces. Cases of internal flow past a sudden increase in a compressible flow are presented by Wick [2]. The flow is first affected upstream. The flow will be affected by the entrance if the flow at the entry is sonic or supersonic. However, the flow will be influenced by the entrance flow when it is subsonic. Second, when the flow in the entrance section is sonic or supersonic, the pressure at the corner is determined by upstream conditions.

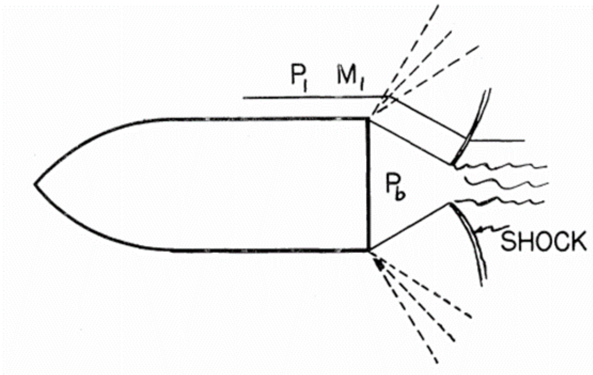

Figure 1. External sudden expansions flow [2].

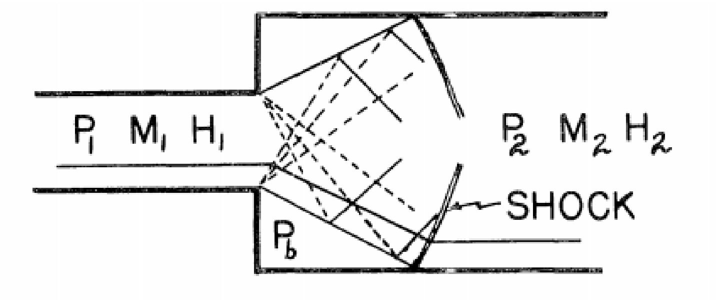

Figure 2. Internal sudden expansions flow [2].

Wick [2] discusses the differences and similarities of the two types of flow described earlier. The only difference between internal and external flow is the wall shear stresses in the wake and the reattached boundary layer in the internal flow. The pressure gradients of parallel wall sections change as the internal flow of the sudden expansion changes. Furthermore, the intersection of the jet boundary will be in the form of Mach lines, with the expansion waves originating from the opposite corner in the internal flow. The wake region, which exists in both flows, is the only similarity.

The developed module is based on the assumption of steady, one-dimensional, isentropic flow. There is no heat exchange within the control volume of isentropic flow, and viscous losses are negligible. However, boundary layers, wakes, and shockwaves are taken into account. When the flow of the free-stream Mach number changes to one, a critical condition occurs. The actual situation happened at the nozzle throat. When the initial flow is supersonic, the normal shock wave is formed due to a spontaneous change in the flow as the velocity decreases and the pressure rises. As the pressure after the shockwave rises, the supersonic effect will be terminated. Concurrently, the velocity falls, and the subsonic flow continues until the backpressure equals the ambient pressure. By lowering the back pressure below the throat pressure, a supersonic region develops downstream at the throat. The shockwave may reoccur at the divergent part, and the subsonic flow will continue. The backpressure is then reduced further until the shockwave moves down the divergent portion of the nozzle.

LITERATURE REVIEW

The nozzle exit area for supersonic flow is classified into three states: over-expanded, fully-expanded, and under-expanded. The fully expanded case is the nozzle exit design condition. The flow is over-expanded when the exit to atmospheric pressure ratio is less than one. The flow is under-expanded when the exit pressure to atmospheric pressure ratio is more significant.

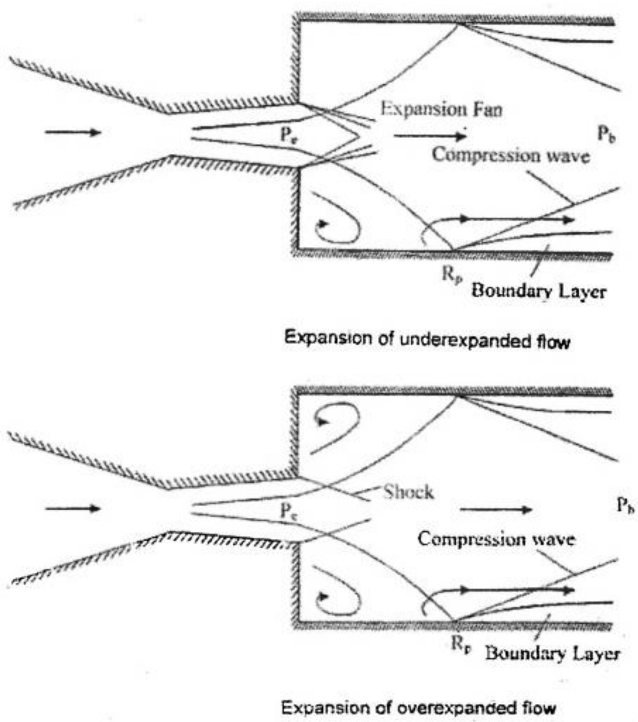

Figure 3. Flow field in the enlarged duct [3]

Pandey and Rathakrishnan [3] investigated the expansion flow in over-expanded and under-expanded cases. Both cases occur at supersonic speeds—an expansion fan formed at the convergent-divergent nozzle exit in an under-expanded flow case. As a result of the earlier reattachment, the reattachment length is reduced. Then, in the case of an over-expanded flow, an oblique shock wave formed at the nozzle exit. As a result of the delayed shocks, the reattachment time will be longer. The vortices formed inside the region between the base and the reattachment point will create a suction force in both cases. The suction force's strength is proportional to the length of the reattachment; the shorter the length, the greater the vortices' power.

Wick [2] defined the base pressure as the internal or external downstream flow pressure. When the flow area expands, the jet boundary at the corner will separate the main flow from the wake. The base pressure is regulated using either the active or passive control methods. The external power source is required for active flow management because it can be turned on and off. However, the procedure necessitates additional time and money. There is a need to change the geometry of the enlarged duct for passive flow management, such as adding ribs or cavities. The device is always operational, which is an added benefit. Passive flow control methods improve the condition of flight vehicles by manipulating the flow characteristics in the boundary layer. Flow manipulation is an efficient way to control mixing in the separated shear layer. Nusselt [4], the first researcher to conduct experiments with the high-velocity gas flow through sudden expansion, based his findings on three conditions. If the entrance velocity is subsonic, the base pressure equals the entrance pressure for starters. Second, if the entrance flow is supersonic, the base pressure may equal, be less than, or be greater than the entrance pressure. Third, the expansion waves from the opposite corner do not affect the jet region if the entrance Mach number is unity.

Korst [5] investigates the base pressure in a transonic and supersonic flow where the flow enters the base after the wake is either sonic or supersonic. He developed a physical flow model based on free stream and mass conservation in the separated zone. He also looked into the impact of mass bleed in the wake. As a result, the findings were very similar to Wick's. Anderson and Williams [6] reported the findings of their study on base pressure and noise caused by air expanding suddenly in a cylindrical duct. First, the duct-to-nozzle area ratio and nozzle geometry determine the minimum base pressure value. Second, at jet pressures roughly equal to those required to produce minimum base pressure, overall noise is at a minimum. At jet pressure, overall noise is minimal, approximately equivalent to that needed to make minimum base pressure.

Cavities can be active, passive, reactive, continuous, or discontinuous. According to Asadullah et al. [8], the complexity of cavity flow necessitates understanding the method within and around it and its effect on base pressure and a multidisciplinary approach. This concept aims to create a convenient pressure gradient by trapping two counter-rotating vortices inside the cavities. These trapped vortices over the suction surface will create a different low-pressure region, resulting in less drag. The presence of cavities boosted the lift-to-drag ratio. For a nozzle’s sudden expansion duct flow control, a static cylinder has been used in recent years shows promising results in controlling base pressure flows for supersonic flow regimes [9]. They conducted several experiments for each expanded condition, such as over, perfectly, and under expanded supersonic regimes at Mach number 2.0 with a sudden expansion duct of the area ratio of 9. The semi-circular grooved cavity in BFS was developed to control the separated flow [10] to reduce drag. The investigation also found the effects of single & multiple cavities [11]. Passive control of base drag in compressible subsonic flow using dimple [12] and multiple cavity [13].

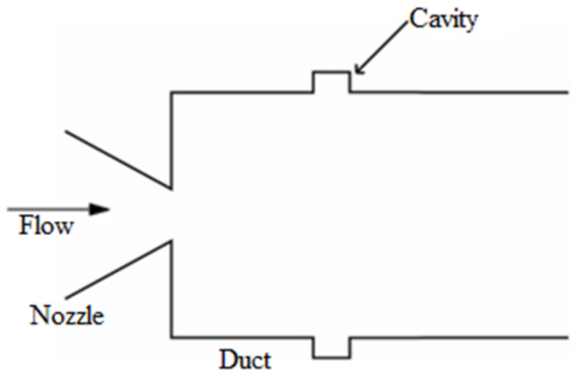

Figure 4. Cavities in enlarged duct [9]

Tanner [14] investigated the base cavity at incidence angles ranging from 0° to 25°. The experiment was based on the investigation, the results gathered for the base cavity at angles of incidence influenced by tail surfaces on base pressure. He concludes that the cavity base's base pressure coefficient is greater than the standard base's. As a result, the base pressure coefficient for the cavity base is more significant than it would be without the cavity base. According to Tanner [14], Morel also discussed the base pressure at zero angle incidence as influenced by the base cavity depths, T/D. The base pressure coefficient decreases as the depth of the base cavity increases. As a result, a base cavity could increase base pressure in axisymmetric flow while decreasing base drag.

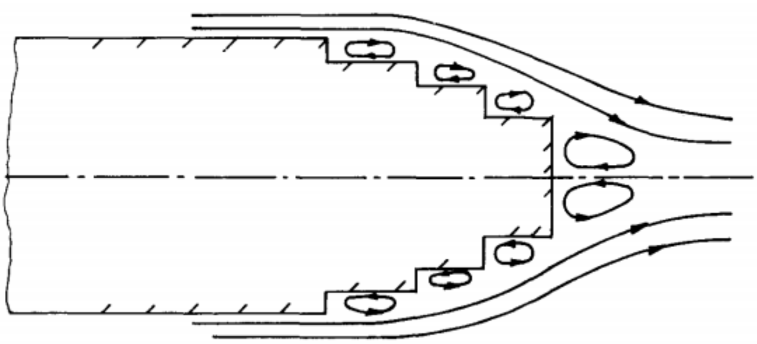

Figure 5. Sketch of a multi-step afterbody [11]

The flow characteristics of a multi-step after-body were studied by Viswanath [15]. Afterbody boat-tailing can reduce drag. However, the afterbody shape was chosen to determine the amount of drag reduction. The flow past a multi-step afterbody was influenced by separated flow at the steps and base in the flow field at Mach 2. The boundary layer separation-reattachment processes influenced the base flow, resulting in distortion effects in the turbulent boundary layer before the base. The length influenced the recovery of a turbulent layer, contributing to the step's separation conditions and height ratio. Afterbody boat-tailing is one of the most effective ways to reduce the base drag of blunt bases. A disc is used to regulate flow downstream of a blunt base. According to Viswanath [16], it results in a smooth flow in the near wake with a vortex located between the base and the disc. A blunt-nose cylinder's forebody drag can also be reduced by installing a disc with a smaller diameter in front at a distance. The drag of the body-disc combination is influenced by several factors, including the base diameter, disc diameter, disc thickness, spindle diameter, and length between the base and the disc. The shape of the disc's rim will also impact the drag. In other words, a stable vortex trapped between the cylinder's base and the disc contributes to the smooth flow of the cylinder-disc combination.

Mair [17] demonstrated the reduction in drag for typically locked vortex afterbodies at low speeds. He explained that the body-disc configuration could experience a drag spike for a specific combination of disc diameter and spacing due to the highly unsteady nature of the near-wake flow. An unstable vortex trapped between the base and the disc is the cause of this condition. According to Rathakrishnan [18], the presence of secondary circulation in the enlarged duct reduces the oscillatory effect of the flow. As a result, the flow will develop smoothly from the base pressure. As a result, when compared to the plain passage, passive controls in the form of annular ribs will significantly reduce base pressure. The base pressure is optimal when the annular ribs aspect ratio is 3:1. Ribs with aspect ratios of 3:2 and 3:3 will increase the base pressure. The aerospikes can synchronize the pressure for subsonic to sonic Mach numbers to control the base pressure in the CD nozzle [19].

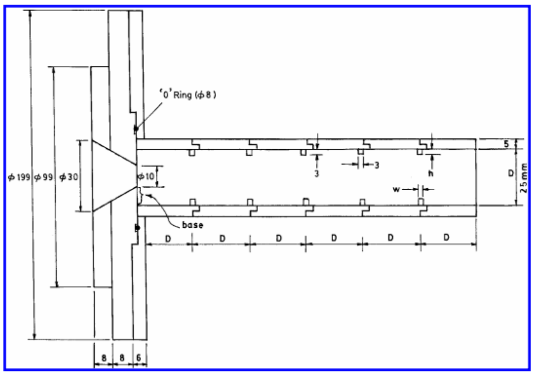

Figure 6. Experimental model with ribs [15]

On the other hand using tiny jets controller in sudden expansion duct several studies have been found in base pressure control in recent years [20]–[35] using an experimental approach as well as numerical simulations [36]–[44]. The CFD study shows an area ratio of sudden expansion duct with different flow-field contours in detail [45]. In some cases, the CFD approach compared with experimental results to find the accuracy in results for such studies of passive control with rectangular rib [46] in the blunt base of the convergent nozzle. This trend continues even when the jets are under-expanded due to the vast area ratio of the enlarged duct [47]. The CFD study shows an area ratio of sudden expansion duct with different flow-field contours in detail [48], [49]. Turbulence modeling is a critical part of the fluent study; for compressible flows, a density-based model has been found in most cases [50]–[52]. Also, the result showed different expansion corners of the duct. It concluded that an isolator with one expansion corner was more efficient in achieving a high static pressure rise [53]. Influence of micro jets on the flow development in the enlarged duct at supersonic Mach number. Additionally, the CFD method was used to investigate external flow formation over different types of airfoil like NACA 2014 [56], CH10 [57], and wedge [58], [59]. The flow control method in a bluff body was also found using non-circular in a front face [60], [61] and splitter plate [62], [63] with the CFD approach.

Also, the data optimization techniques has made the attenstion in solving such probelms of mechanical engineering using the analysis such as clustering analysis, heat maps are used to envisage the enormous data from wind tunnel tests results by Asif et al. [64], [65]. They mentioned that back-propagation models (BPMs) are established on input and output options to forecast the pressure at large Mach numbers. Based on their results, the BPMs with 2- hidden layers with four neurons per layer are highly appropriate for the relapse analysis. Quadros et al. [66] used CFD simulations of turbulent supersonic flow results to form relations between input and output of the Mamdani-based fuzzy logic approach. Triangular, generalized bell shape and Gaussian membership functions. With these previous studies, it can be realized that the fuzzy logic technique will help determine the parameters in pressure base control.

METHODOLOGY

ANSYS Workbench, based on Fluid Flow (Fluent) analysis systems, was used for the entire process's Computational Fluid Dynamics (CFD) software. Figure 7 depicts an axisymmetric C-D nozzle connected to a circular duct and an annular rectangular cavity. Based on the experimental setup by Pandey and Rathakrishnan [3], the dimensions for the convergent-divergent nozzle with suddenly expanded circular are as follows.

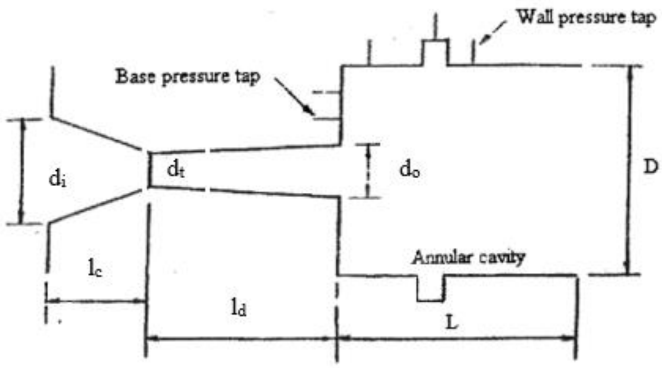

Figure 7. Converging diverging nozzle model suddenly expanded into a duct with an annular cavity

The current work has a Mach number of 1.8. The duct diameter is fixed at D = 16 mm, and the duct length, L, varies according to the L/D ratio. The nozzle inlet has a diameter of 22.34 mm, and the nozzle outlet has a diameter of 10 mm. The convergent angle, θ_c, is 15 degrees, and the divergent angle, θ_d, is 5 degrees. Two-cavity aspect ratios were used in this study. The aspect ratio is defined as the cavity width to cavity height ratio. The cavity aspect ratio one dimension is 3:3, and the cavity aspect ratio 2 is 6:3—the L/D ratio, which ranges from 1 to 10. After creating the domain geometry with Design Modeler, the next critical step is mesh generation. This section divides the domain geometry into smaller and non-overlapping subdomains to solve the flow physics within the domain geometry. The essential fluid flows are numerically solved to determine the discrete values of flow properties such as velocity and pressure, according to each mesh of cells in the domain geometry. According to Koomullil et al. [67], mesh generation can be classified into two types based on the topology of the domain elements: structured meshes and unstructured meshes. The mesh in this project is generated automatically using the Quadrilateral Dominant method. This method ensures that the element's size is symmetrical throughout the geometry.

The assumptions are made to mimic the flow behavior with the exact physical situation and ensure that the numerical simulation methods compromise the actual physical condition. The continuity equation, also known as the conservation of mass equation, can be defined as follows:

$$\frac{\partial \rho}{\partial t} + \nabla . (\rho V) = 0 \tag{1}$$

In the Cartesian coordinate system, the continuity equation can be written as:

$$\frac{\partial \rho}{\partial t} + \rho \left(\frac{\partial u}{\partial x} + \frac{\partial v}{\partial y} + \frac{\partial w}{\partial z} \right) = 0 \tag{2}$$

The first assumption is a steady-state two-dimensional flow because the flow is symmetric along the flow direction. The fluid is compressible, according to the second assumption. These two assumptions are as follows:

$$\frac{\partial \rho}{\partial t} + \rho \left(\frac{\partial u}{\partial x} + \frac{\partial v}{\partial y} \right) = 0 \tag{3}$$

ρ is the density of the flow, u is the velocity in the x-direction, and v is the velocity in the y-direction. Equation (3) can be written in a cylindrical coordinate system:

$$\frac{1}{r}\frac{\partial (\rho r u)}{\partial r} + \frac{\partial (\rho v)}{\partial z} = 0 \tag{4}$$

r is the radius in the z-direction, u is the velocity in the z-direction, and v is the velocity in the y-direction. The gas density is a variable when the Mach number is more significant than 0.3 compressible flow analysis. As a result, the ideal gas constant is chosen. The third assumption is that the velocity flow is turbulent. Turbulence happens when there are random fluctuations in the fluid. As a result, the k-epsilon (k-) turbulence model is employed. This model is used in flow situations to provide economy, robustness, and sufficient accuracy. The turbulent kinetic energy (k equation) can be expressed as follows:

$$\frac{\partial(\rho uK)}{\partial z}+\frac{1}{r}\frac{\partial(\rho vK)}{\partial r}\frac{\partial}{\partial z}\left[\left(\mu+\frac{\mu_t}{\sigma_k}\right)\frac{\partial K}{\partial z}\right]+\frac{1}{r}\frac{\partial}{\partial r}\left[r\left(\mu+\frac{\mu_t}{\sigma_k}\right)\frac{\partial K}{\partial r}\right]\rho\varepsilon+G \tag{5}$$

σ_k is the turbulent Prandtl number for K, ε is the turbulent kinetic energy dissipation rate, and G is the turbulence generation term. G can be written as:

$$G=\mu_t\left(\frac{\partial u_i}{\partial x_j}+\frac{\partial u_j}{\partial x_i}\right)\frac{\partial u_i}{\partial x_j}-\frac{2}{3}k\delta_{ij}\frac{\partial u_i}{\partial x_j} \tag{6}$$

The kinetic energy of turbulence dissipation (ε equation) can be described as:

$$\frac{\partial(\rho u\varepsilon)}{\partial z}+\frac{1}{r}\frac{\partial(\rho v\varepsilon)}{\partial r}=\frac{\partial}{\partial z}\left[\left(\mu+\frac{\mu_t}{\sigma_\varepsilon}\right)\frac{\partial\varepsilon}{\partial z}\right]+\frac{1}{r}\frac{\partial}{\partial r}\left[r\left(\mu+\frac{\mu_t}{\sigma_\varepsilon}\right)\frac{\partial\varepsilon}{\partial r}\right]-C_1f_1\left(\frac{\varepsilon}{K}\right)G-C_2f_2\left(\frac{\varepsilon^2}{K}\right) \tag{7}$$

μ_t is the turbulent viscosity, C_1, C_2, f_1, f_2, σ_ε and μ_t are arbitrary constants for the kinetic energy of turbulence dissipation model in Equation (6) and Equation (7). The fourth assumption is that fluid viscosity is a function of temperature. The law of Sutherland was chosen as the dynamic viscosity. Sutherland's viscosity model based on three coefficients is defined as:

$$\mu=\mu_0\left(\frac{T}{T_0}\right)^{3/2}\frac{T_0+S}{T+S} \tag{8}$$

μ is the viscosity, μ_0 is the reference viscosity, T is the static temperature, T_0 is the reference temperature, and S is the Sutherland constant. The last assumption is the flow exits from the duct at ambient atmospheric pressure.

The mesh independence test was performed to determine the best grid size. This is because higher NPR necessitates more iterations and a longer computing time. Selecting the appropriate element size can obtain higher accuracy with less computing time. In general, 10k iterations are sufficient for the solutions to converge, but the iterations are set to 20k to ensure that the solutions converged correctly. The element size is varied several times to ensure that the solution converges. After a mesh independence check with three different element sizes, the element size 0.1 mm with nodes around 50353 and the number of elements 49594 was chosen, as shown in Figure 8.

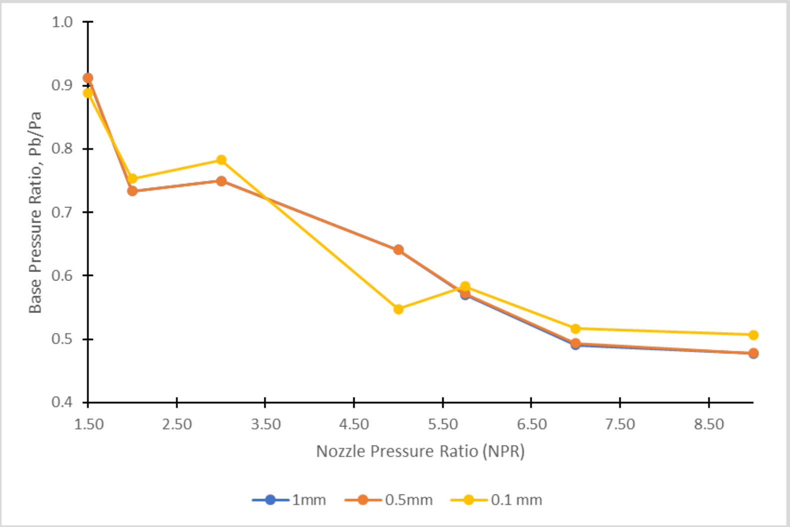

Figure 8. The base pressure for different element sizes having converged values

NPR (P01/Pa) 2.10 was chosen from Pandey and Rathakrishnan's [3] previous paper to compare the current work. This geometry validation aims to simulate the theoretical flow parameters for the model with cavity aspect ratio

1 using CFD simulation (ANSYS Fluent) in 2D modeling. For verification, the current work's L/D was varied from 2 to 10.

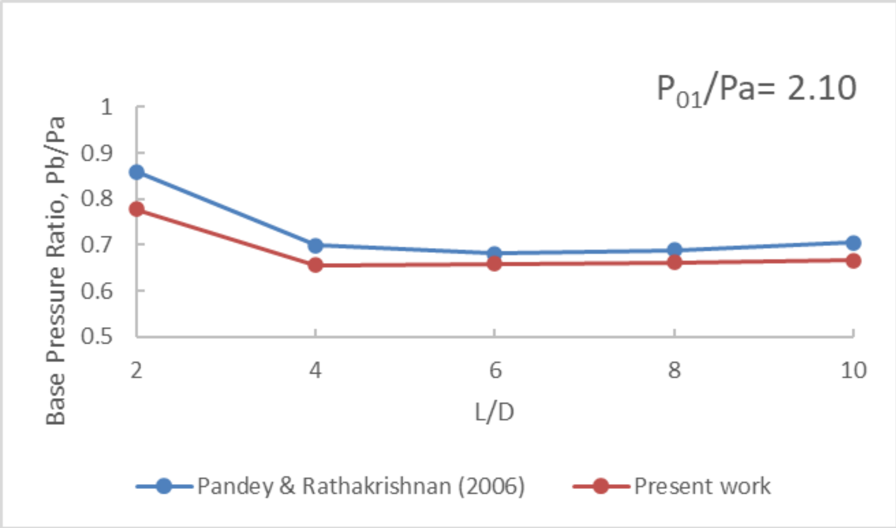

Figure 9. Verification of present work.

Figure 9 depicts the curves of current and previous work data. The curves all follow the same pattern, and each point is close to the one before it. The percentage error was calculated as well. The current work had a percentage error of less than 10% compared to the previous work. As a result, the recent work's validation was successful.

RESULTS AND DISCUSSION

Figure 10 depicts the base pressure for a plain duct and an enlarged duct with a cavity at L/Ds ranging from 1 to 10. The base pressure for the plain duct is the lowest compared to the dilated duct with control (as shown by the dark blue line). However, the main focus is on discussing the results related to the base's location. As shown in Figure 10, the light blue line in Figure 10 (a) for NPR 2 has the highest base pressure ratio compared to the others. So, for L/D 1 to 10, the most efficient cavity location for NPR 2 is 2D from the base. The effective cavity location for NPR 5 varies with L/D, as shown in Figure 10 (b). From L/D 1 to 2, the base pressure decreases. The grey line depicts the efficient location is at 1D from the base. The base pressure is almost constant for all control locations in the duct when L/D is greater than 3. The appropriate cavity location is 0.5D from the base, as indicated by the orange line. The base pressure dropped from L/D 1 to 2 for NPR 5.75, as shown in Figure 10 (c). Then, the base pressure is nearly constant from L/D greater than 2. This demonstrates that the shortest duct length required for the flow to remain attached is L/D = 2. The best cavity location for NPR 5.75 is 0.5D from the base, as shown by the orange line. The base pressure for NPR 7 and NPR 9 changes only slightly from L/D 1 to 10. According to the graph, the orange line has a higher base pressure value. As a result, the effective cavity location for these NPR is 0.5D away from the base wall.

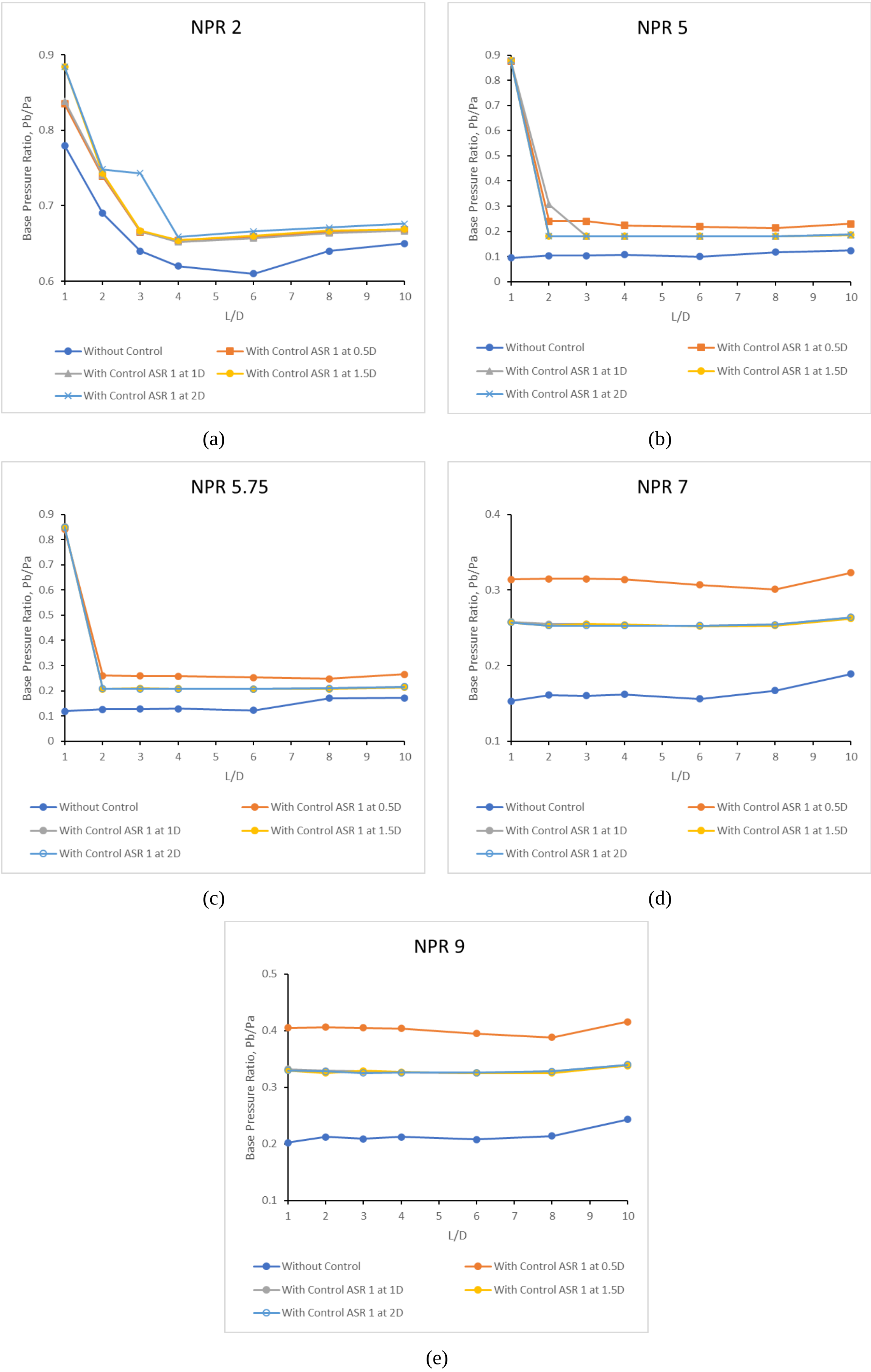

Figure 10. The base pressure ratio variations with L/D for plain duct and duct control at numerous locations.

Figure 11 illustrates the normalized base pressure for a plain duct and an enlarged duct with control at various NPRs. The dark blue color line represents the plain duct base pressure ratio, while the other colors represent control. According to the figures, for NPR less than five nozzles over-expanded, it is difficult to determine which model has the preferred cavity location to obtain the highest base pressure. These findings confirm that the control (either active or passive) is ineffective when nozles are over-expanded. It can also be seen that the base pressure fluctuates inconsistently for all of the L/Ds in this study. However, in this case, the base pressure fell sharply from NPR 2 to NPR 5, except NPR 3 for L/D 1 and 2, as shown in Figures 11 (a) and (b). This decrease in base pressure is related to the degree of expansion as the jets are over-expanded until NPR = 5.75. As the NPR gradually rises, the level of over-expansion decreases, as do the base pressure values.

On the contrary, NPR's base pressure has increased by more than 5. This trend reversal is associated with a shift in expansion levels. Jets were over-expanded until NPR equaled 5. Any NPR greater than 5.75 causes jets to become under-expanded and the nozzles to flow under the influence of a favorable pressure gradient. Control is effective at this NPR and beyond, increasing the base pressure. Compared to other models, the plain duct has the lowest base pressure. Based on Figure 11, the base pressure for the model with an enlarged duct at cavity location 0.5D from the base pressure is the most effective among the other models. This is evident in the orange line plots from the graphs with the highest base pressure ratios compared to other models. According to the graphs in the figure above, the presence of a cavity is effective for higher NPR.

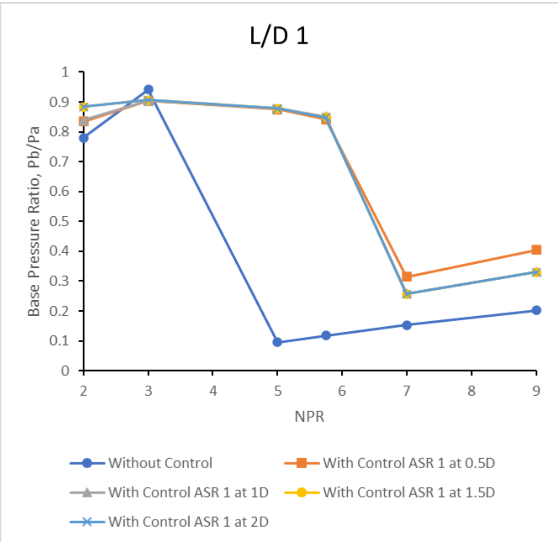

(a)

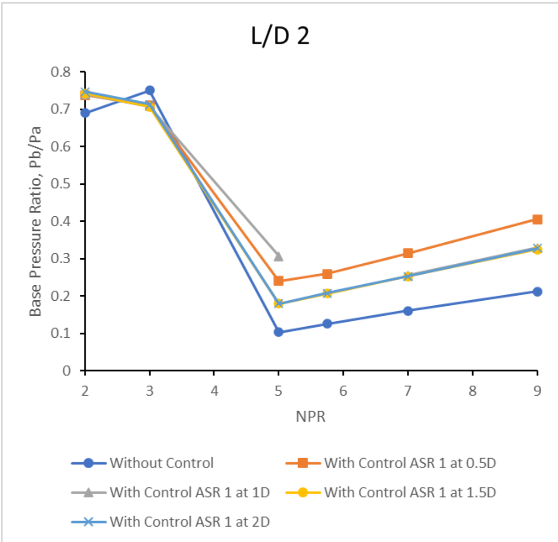

(b)

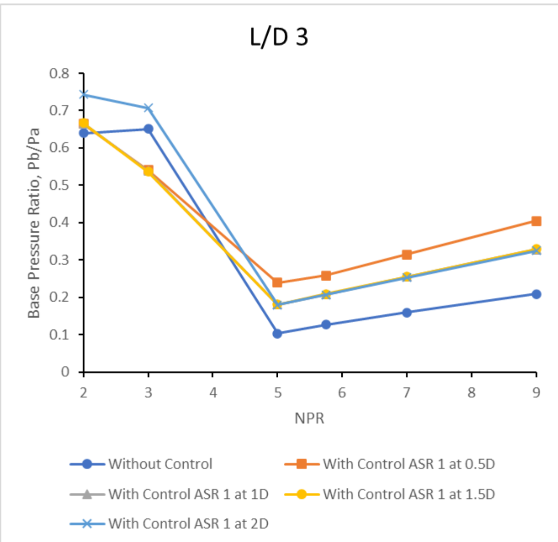

(c)

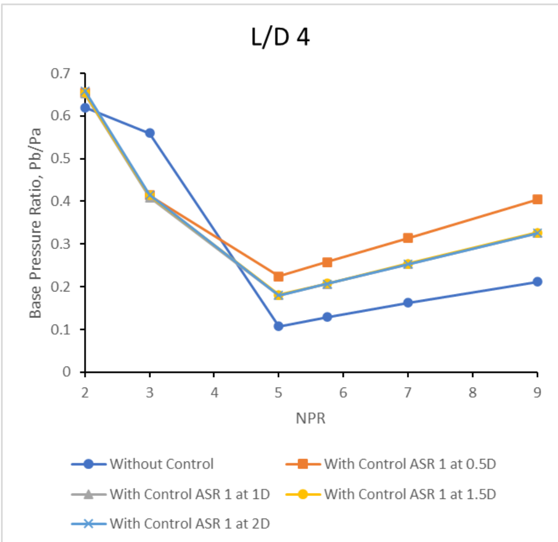

(d)

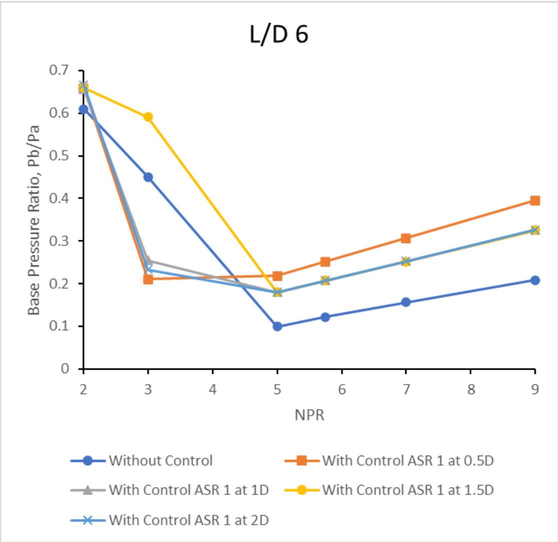

(e)

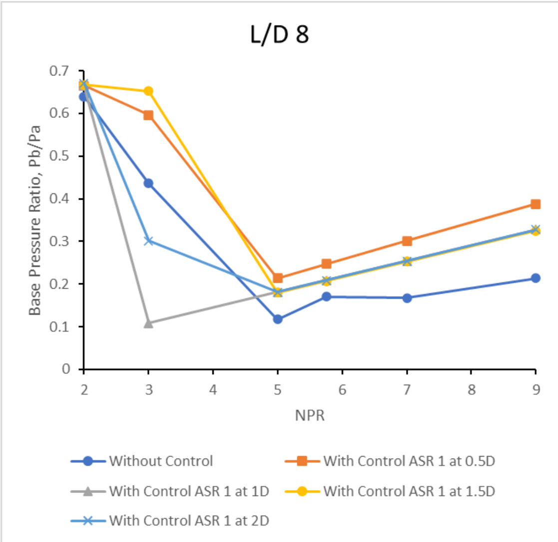

(f)

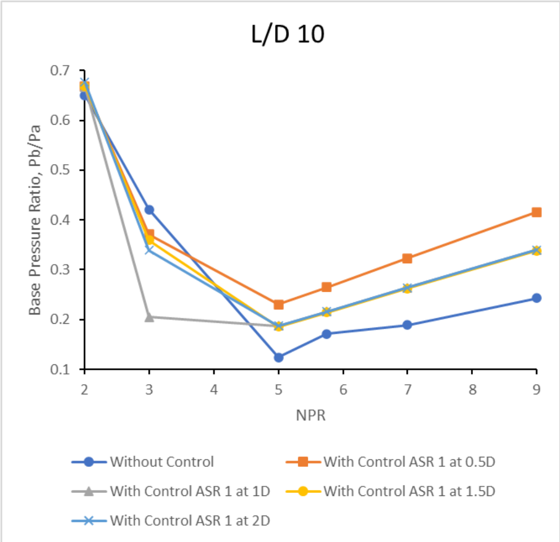

(g)

Figure 11. The base pressure ratio varies with NPR for plain duct and enlarged duct with a cavity.

CONTOURS RESULT FOR C-D NOZZLE EXPANDED SUDDENLY INTO CIRCULAR DUCT WITH CONTROL

The contour results were gathered at various L/D, cavity location, and cavity aspect ratios for Mach number 1.8 with an area ratio of 2.56 and an NPR range of 2 to 9. The current study demonstrates that the presence of a cavity has a significant impact on base pressure. The contour results are classified into five groups, which are as follows:

1. The pressure distribution for the present work model with cavity aspect ratio 3:3 and cavity location 0.5D
2. The pressure distribution for the present work model with cavity aspect ratio 3:3 and cavity location 1D
3. The pressure distribution for the present work model with cavity aspect ratio 3:3 and cavity location 1.5D
4. The pressure distribution for the present work model with cavity aspect ratio 3:3 and cavity location 2D
5. The pressure distribution for the present work model with cavity aspect ratio 3:6 and cavity location 1D

The L/D 1 contour results for Groups 2 and higher are not included because the flow may not be attached to the duct wall. The pressure distribution contours for the C-D nozzle that suddenly expanded into an enlarged duct with the cavity are depicted in the figures below. The maximum pressure value is red, while the minimum pressure value is indicated by dark blue.

Table 1. The model geometry for Group 1 with L/D 1.

Group	1
L/D	1
Duct length	16 mm
Cavity location from the base wall	0.5D (6.5mm)
Cavity aspect ratio	1

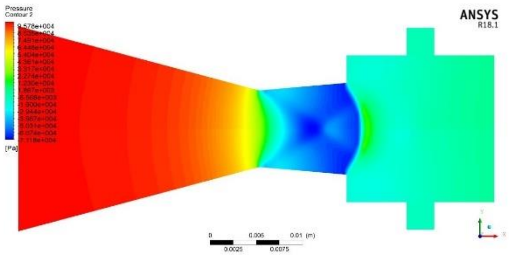

a) NPR 2

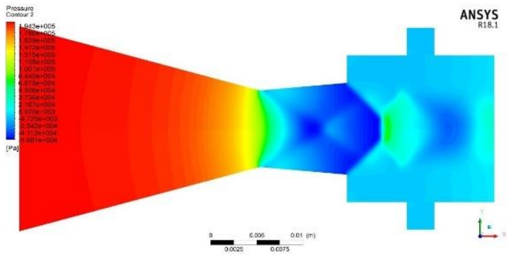

b) NPR 3

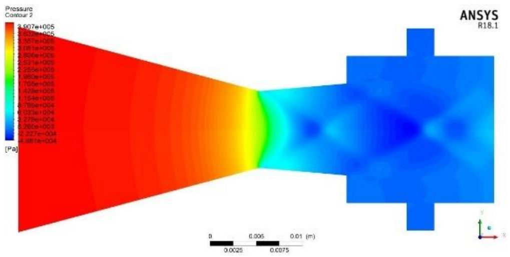

c) NPR 5

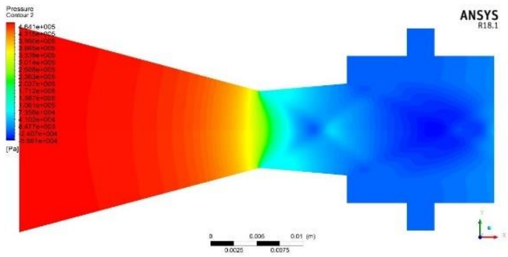

d) NPR 5.75

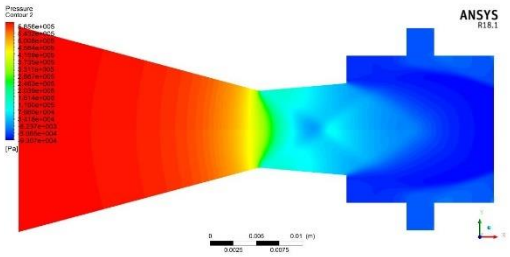

e) NPR 7

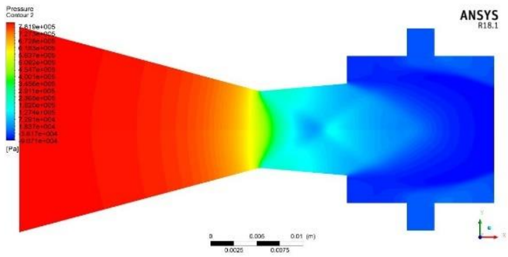

f) NPR 9

Figure 12. The contour results for the model with L/D 1, cavity ASR 1, and cavity location 0.5D.

Table 2. The model geometry for Group 1 with L/D 2.

Group	1
L/D	2
Duct length	32 mm
Cavity location from the base wall	0.5D (6.5mm)
Cavity aspect ratio	1

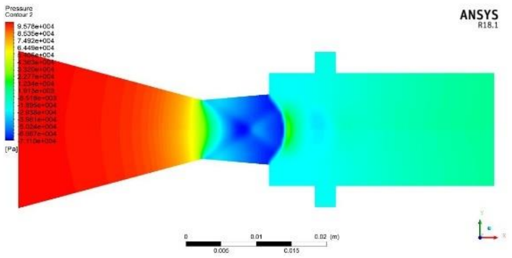

a) NPR 2

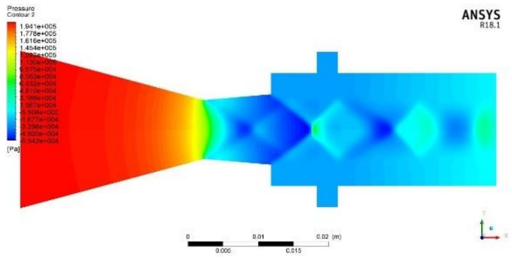

b) NPR 3

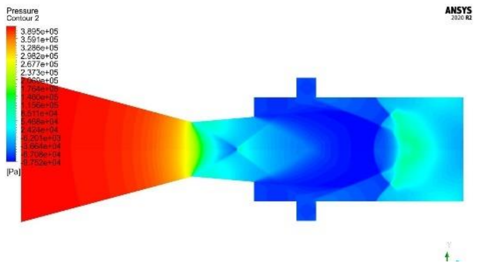

c) NPR 5

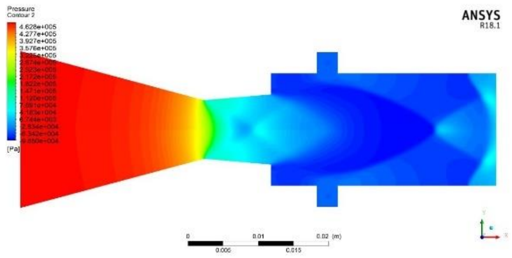

d) NPR 5.75

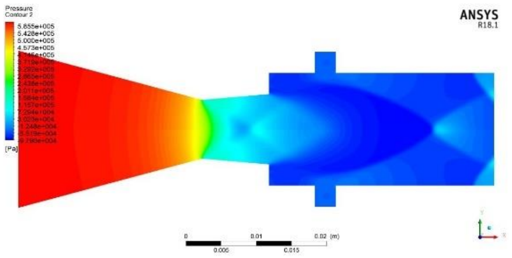

e) NPR 7

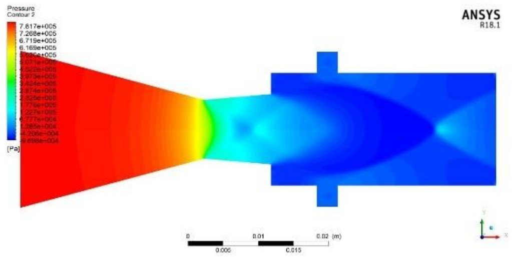

f) NPR 9

Figure 13. The contour results for the model with L/D 2, cavity ASR 1, and cavity location 0.5D.

Table 3. The model geometry for Group 1 with L/D 3.

Group	1
L/D	3
Duct length	48 mm
Cavity location from the base wall	0.5D (6.5mm)
Cavity aspect ratio	1

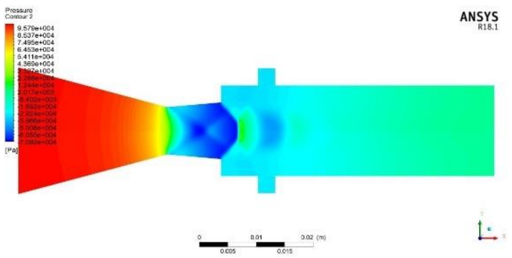

a) NPR 2

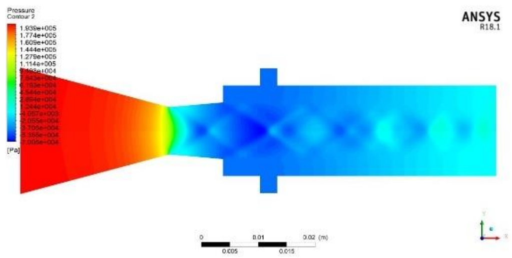

b) NPR 3

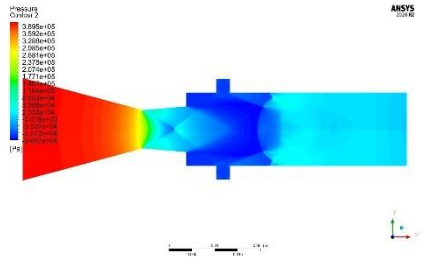

c) NPR 5

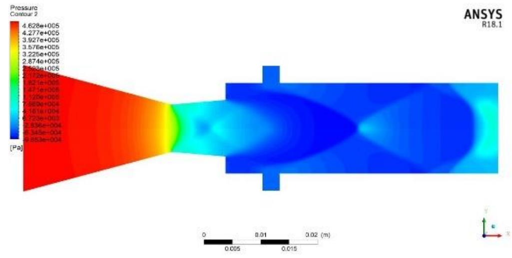

d) NPR 5.75

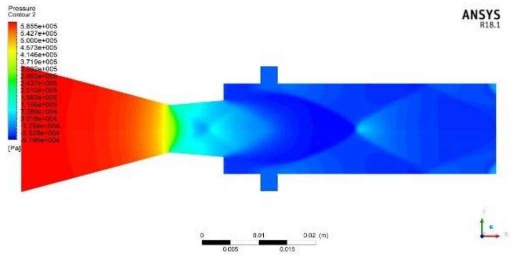

e) NPR 7

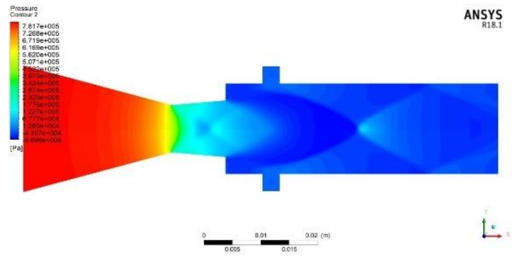

f) NPR 9

Figure 14. The contour results for the model with L/D 3, cavity ASR 1, and cavity location 0.5D.

Table 4. The model geometry for Group 1 with L/D 4.

Group	1
L/D	4
Duct length	64 mm
Cavity location from the base wall	0.5D (6.5mm)
Cavity aspect ratio	1

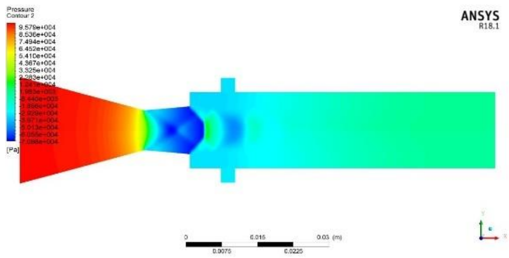

a) NPR 2

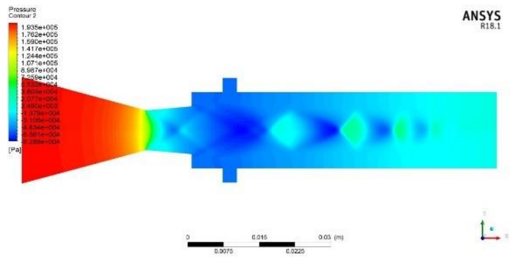

b) NPR 3

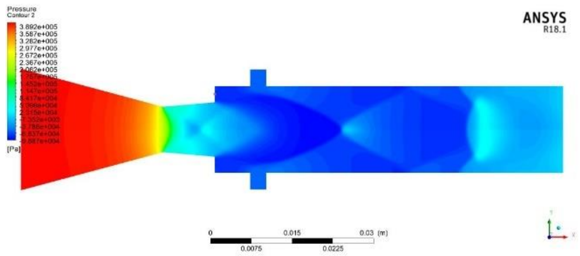

c) NPR 5

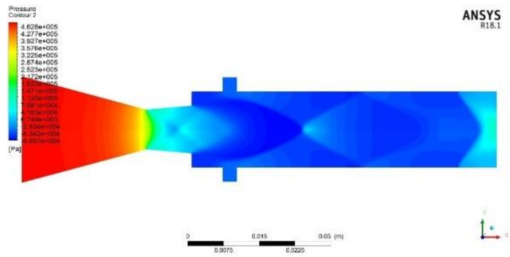

d) NPR 5.75

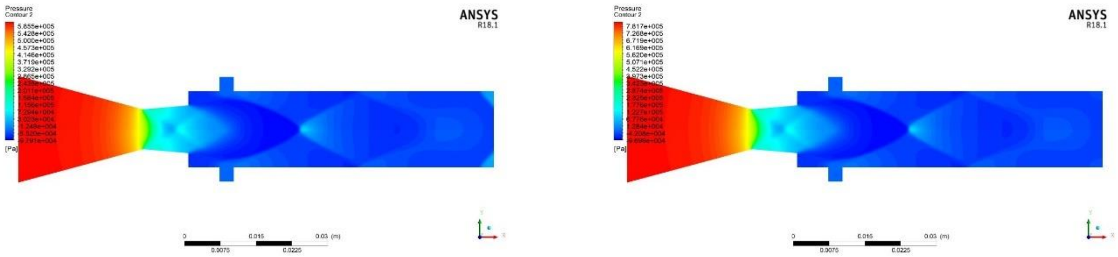

e) NPR 7 f) NPR 9

Figure 15. The contour results for the model with L/D 4, cavity ASR 1, and cavity location 0.5D.

Table 5. The model geometry for Group 1 with L/D 6.

Group	1
L/D	6
Duct length	96 mm
Cavity location from the base wall	0.5D (6.5mm)
Cavity aspect ratio	1

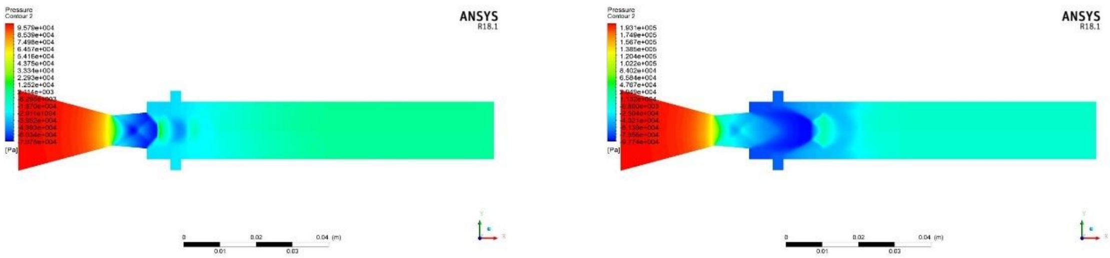

a) NPR 2 b) NPR 3

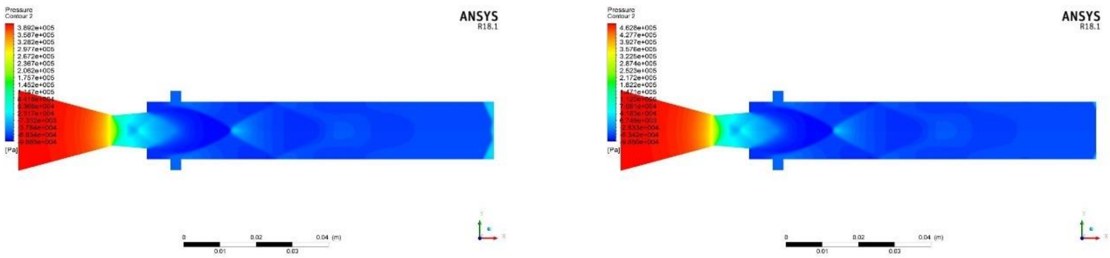

c) NPR 5 d) NPR 5.75

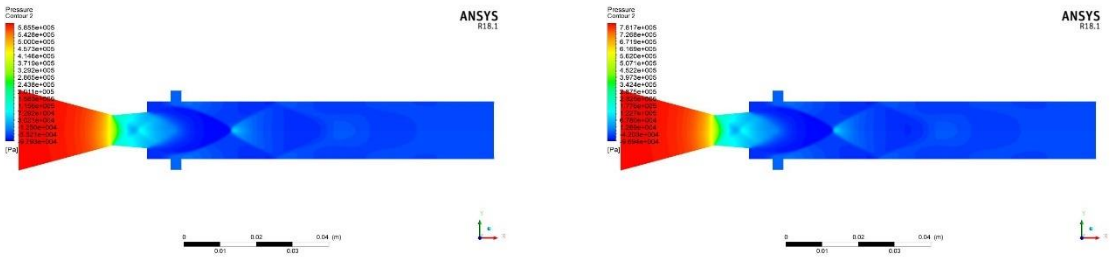

e) NPR 7 f) NPR 9

Figure 16. The contour results for the model with L/D 6, cavity ASR 1, and cavity location 0.5D.

Table 6. The model geometry for Group 1 with L/D 8.

Group	1
L/D	8
Duct length	128 mm

Cavity location from the base wall	0.5D (6.5mm)
Cavity aspect ratio	1

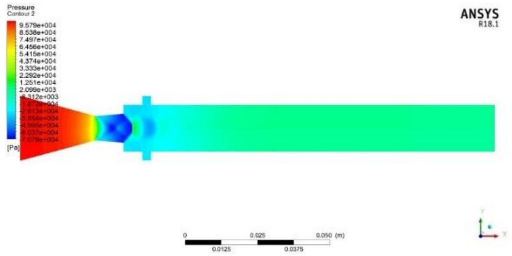

a) NPR 2

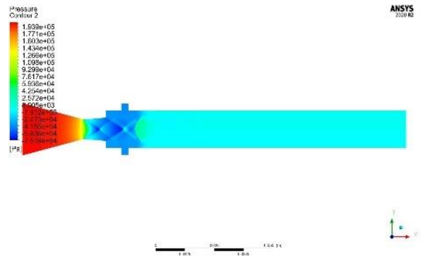

b) NPR 3

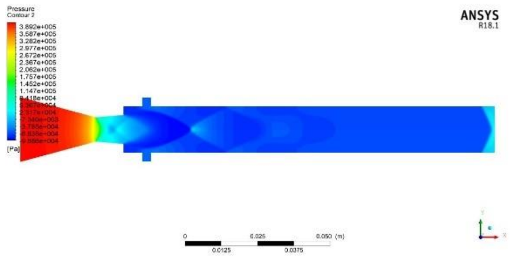

c) NPR 5

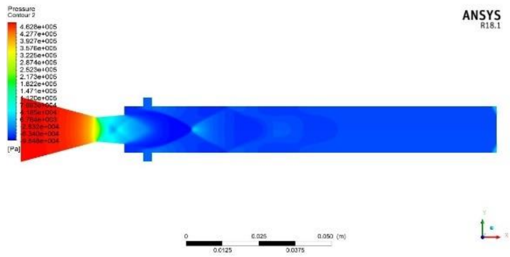

d) NPR 5.75

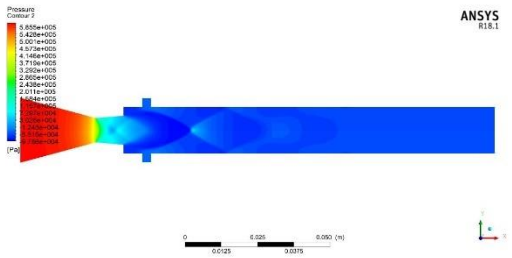

e) NPR 7

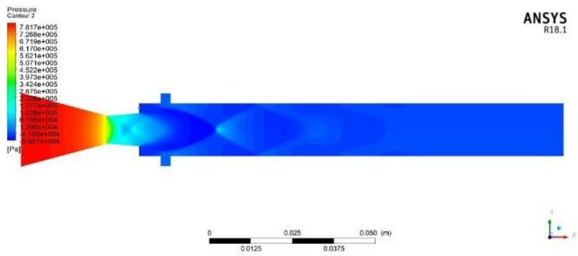

f) NPR 9

Figure 17. The contour results for the model with L/D 8, cavity ASR 1, and cavity location 0.5D.

Table 7. The model geometry for Group 1 with L/D 10.

Group	1
L/D	10
Duct length	160 mm
Cavity location from the base wall	0.5D (6.5mm)
Cavity aspect ratio	1

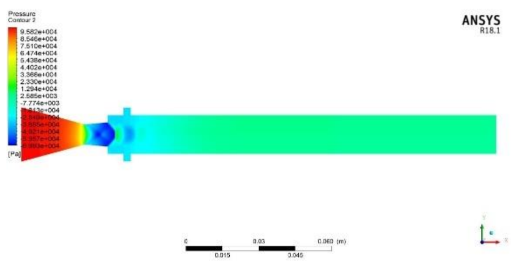

a) NPR 2

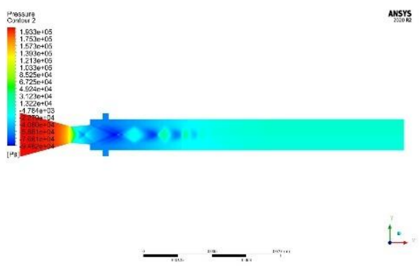

b) NPR 3

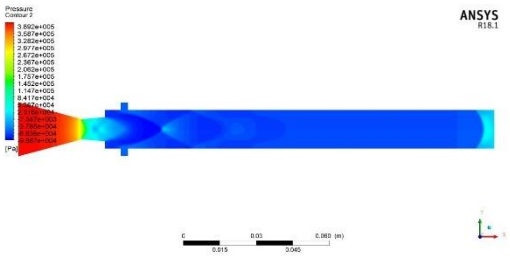

c) NPR 5

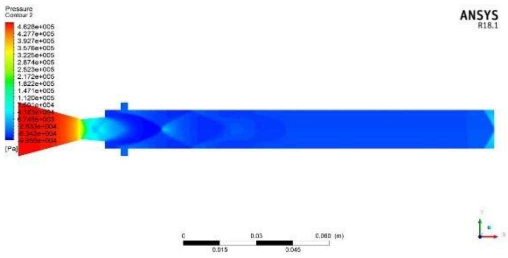

d) NPR 5.75

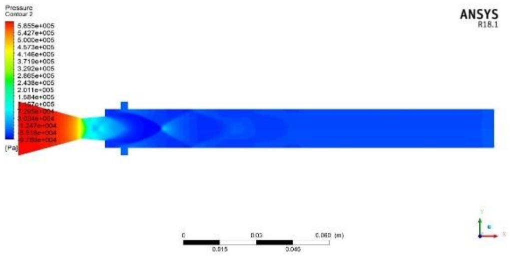

e) NPR 7

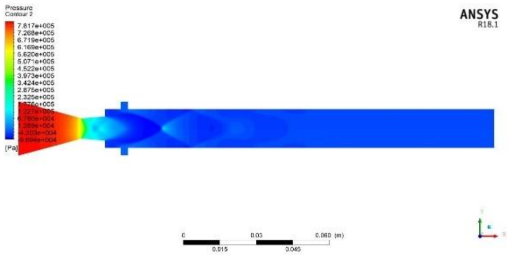

f) NPR 9

Figure 18. The contour results for the model with L/D 10, cavity ASR 1, and cavity location 0.5D.

Table 8. The model geometry for Group 2 with L/D 2.

Group	2
L/D	2
Duct length	32 mm
Cavity location from the base wall	1D (14.5 mm)
Cavity aspect ratio	1

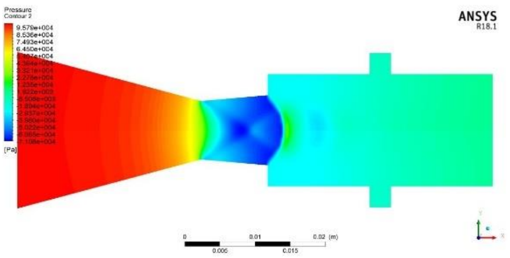

a) NPR 2

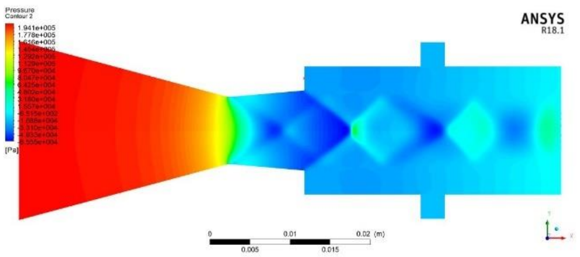

b) NPR 3

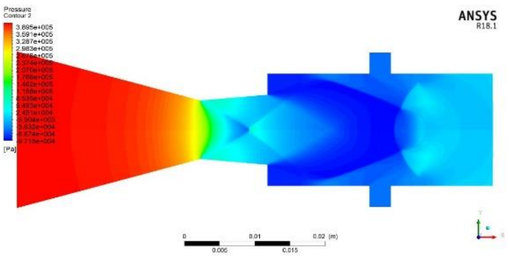

c) NPR 5

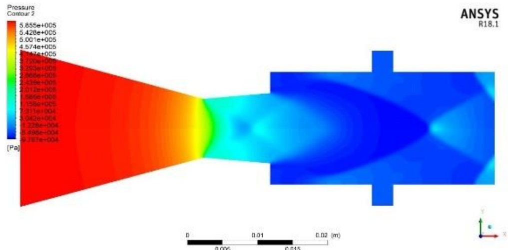

d) NPR 7

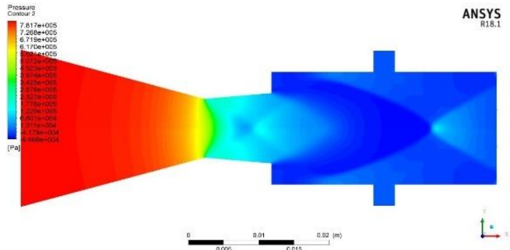

e) NPR 9

Figure 19. The contour results for the model with L/D 2, cavity ASR 1, and cavity location 1D.

Table 9. The model geometry for Group 2 with L/D 3.

Group	2
L/D	3
Duct length	32 mm
Cavity location from the base wall	1D (14.5 mm)
Cavity aspect ratio	1

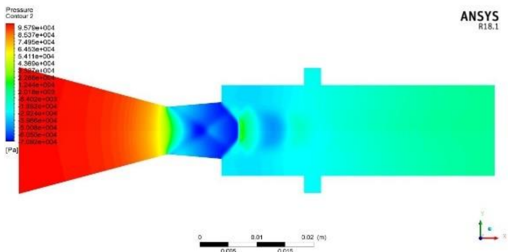

a) NPR 2

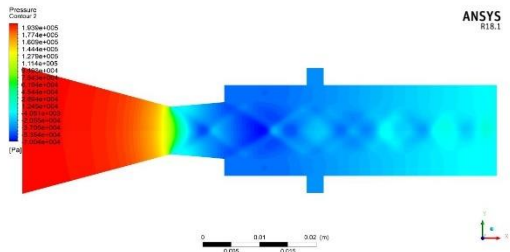

b) NPR 3

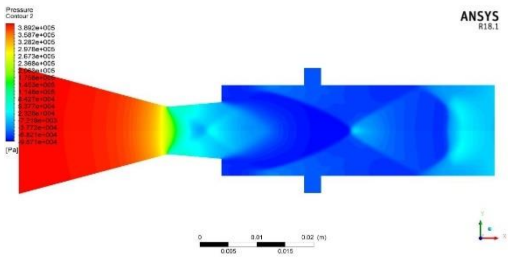

c) NPR 5

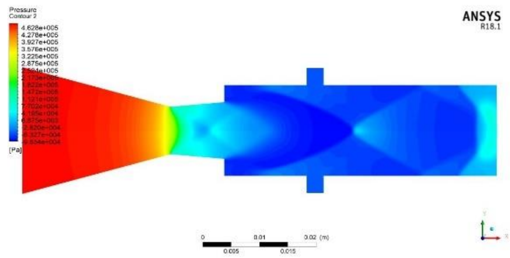

d) NPR 5.75

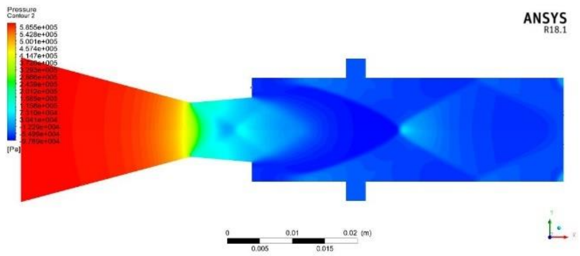

e) NPR 7

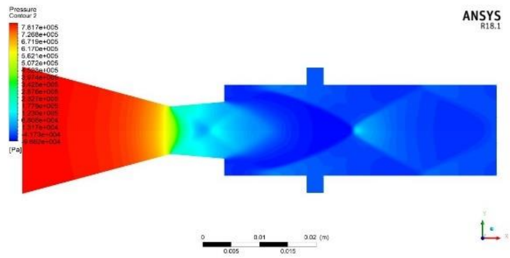

f) NPR 9

Figure 20. The contour results for the model with L/D 3, cavity ASR 1, and cavity location 1D.

Table 10. The model geometry for Group 2 with L/D 4.

Group	2
L/D	4
Duct length	64 mm

Cavity location from the base wall	1D (14.5 mm)
Cavity aspect ratio	1

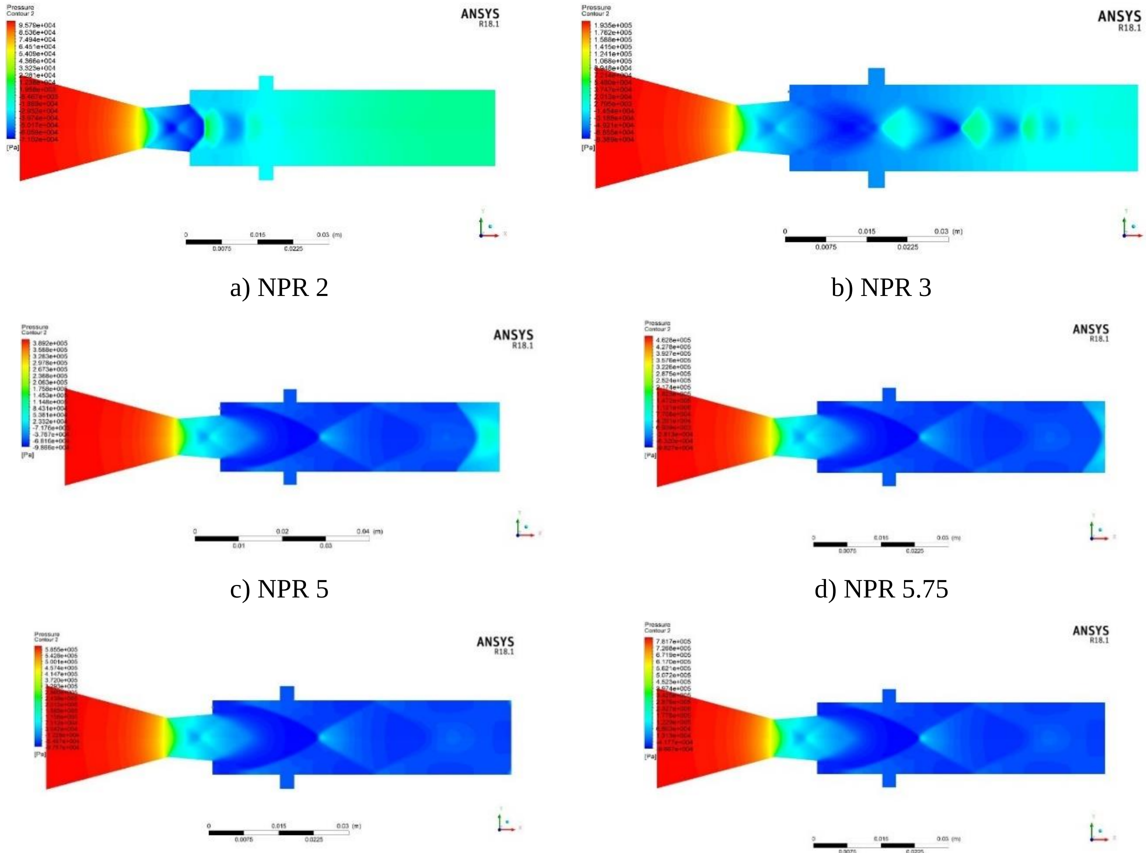

a) NPR 2 b) NPR 3

c) NPR 5 d) NPR 5.75

e) NPR 7 f) NPR 9

Figure 21. The contour results for the model with L/D 4, cavity ASR 1, and cavity location 1D.

Table 11. The model geometry for Group 2 with L/D 6.

Group	2
L/D	6
Duct length	96 mm
Cavity location from the base wall	1D (14.5 mm)
Cavity aspect ratio	1

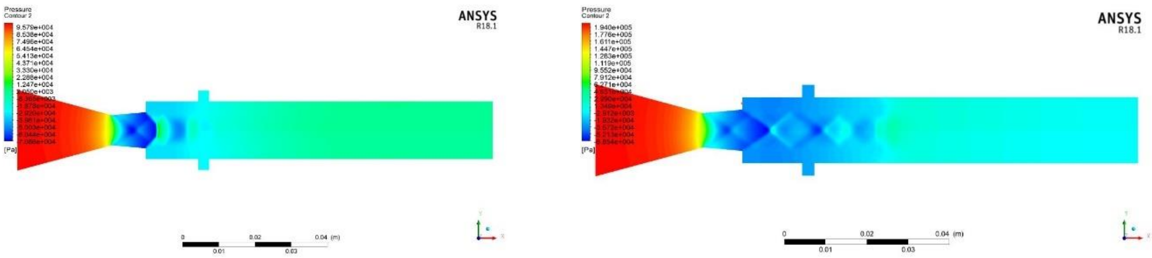

a) NPR 2 b) NPR 3

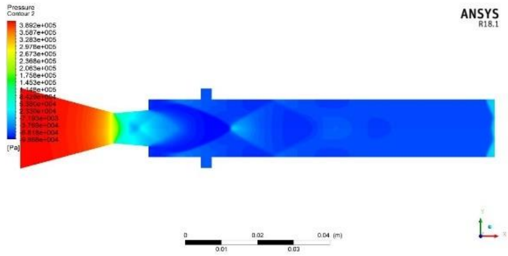

c) NPR 5

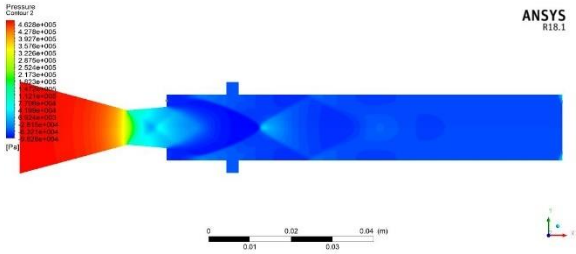

d) NPR 5.75

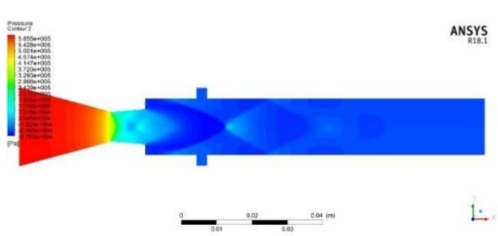

e) NPR 7

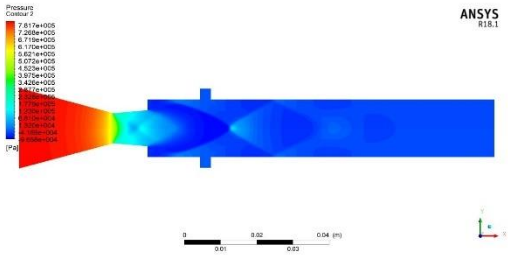

f) NPR 9

Figure 22. The contour results for the model with L/D 6, cavity ASR 1, and cavity location 1D.

Table 12. The model geometry for Group 2 with L/D 8.

Group	2
L/D	8
Duct length	128 mm
Cavity location from the base wall	1D (14.5 mm)
Cavity aspect ratio	1

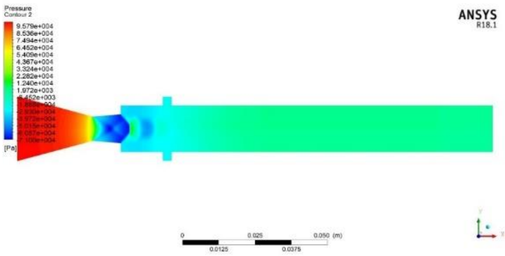

a) NPR 2

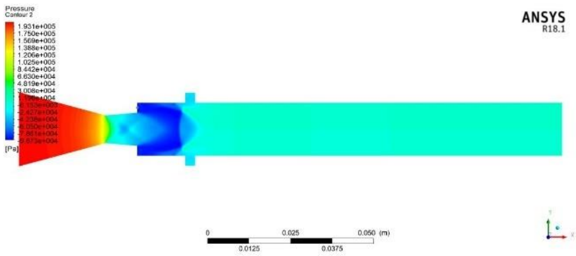

b) NPR 3

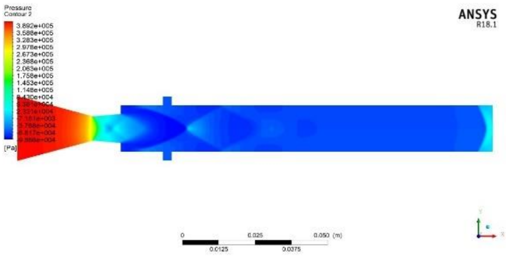

c) NPR 5

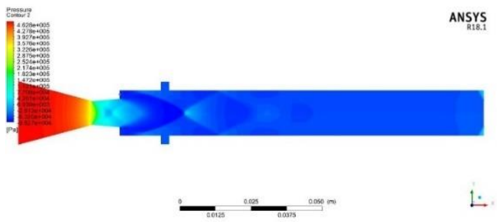

d) NPR 5.75

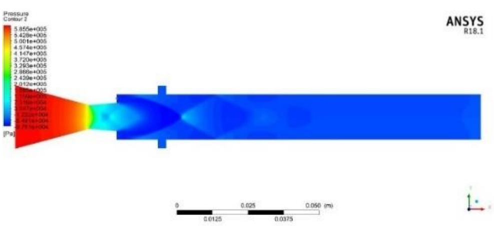

e) NPR 7

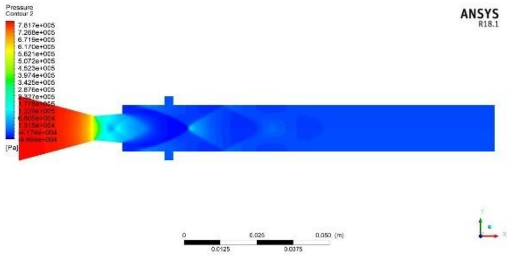

f) NPR 9

Figure 23. The contour results for the model with L/D 8, cavity ASR 1, and cavity location 1D.

Table 13. The model geometry for Group 2 with L/D 10.

Group	2
L/D	10
Duct length	160 mm
Cavity location from the base wall	1D (14.5mm)
Cavity aspect ratio	1

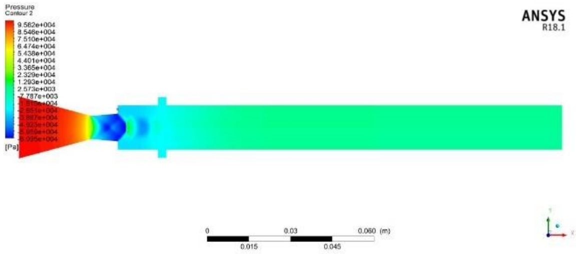

a) NPR 2

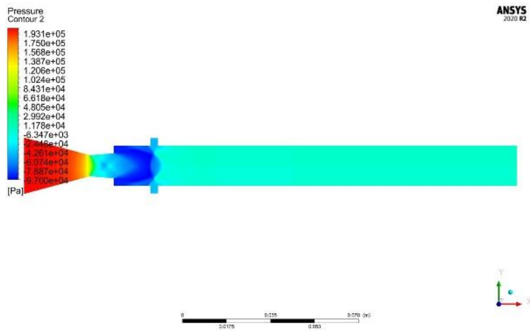

b) NPR 3

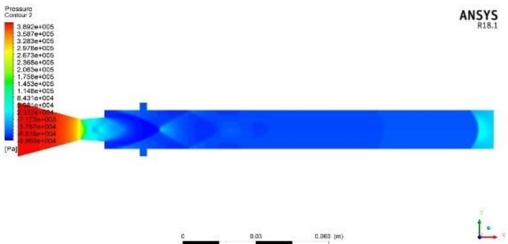

c) NPR 5

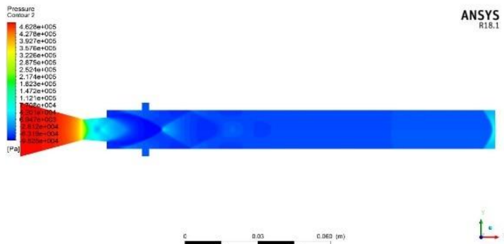

d) NPR 5.75

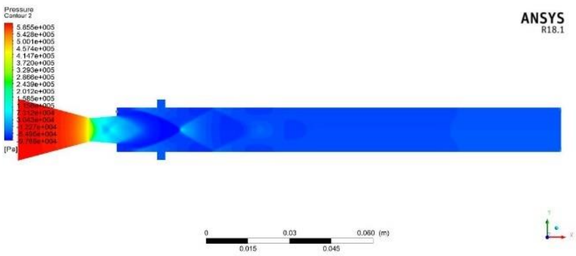

e) NPR 7

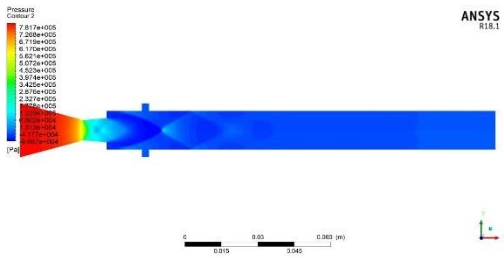

f) NPR 9

Figure 24. The contour results for the model with L/D 10, cavity ASR 1, and cavity location 1D.

Table 14. The model geometry for Group 3 with L/D 2.

Group	**3**
L/D	2
Duct length	32 mm
Cavity location from the base wall	1.5D (22.5mm)
Cavity aspect ratio	1

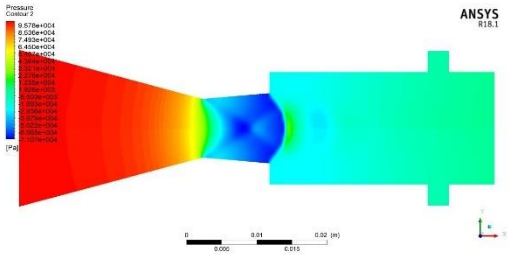

a) NPR 2

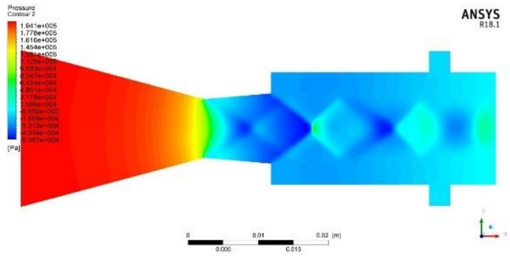

b) NPR 3

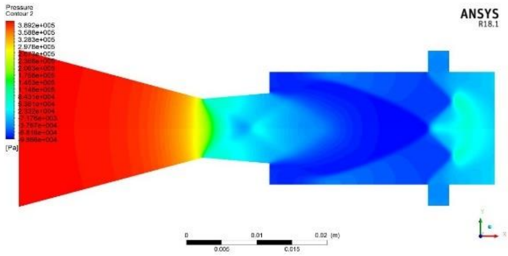

c) NPR 5

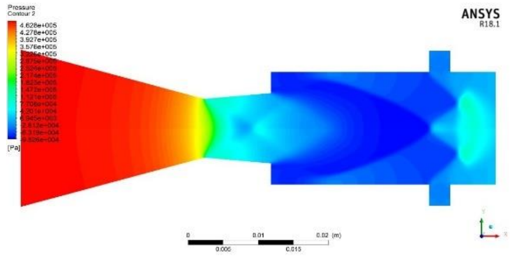

d) NPR 5.75

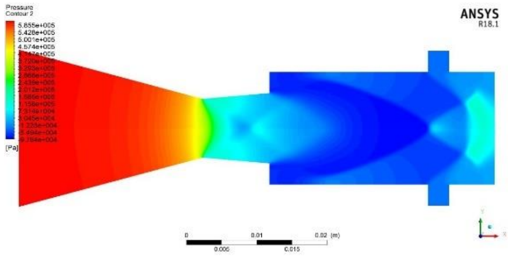

e) NPR 7

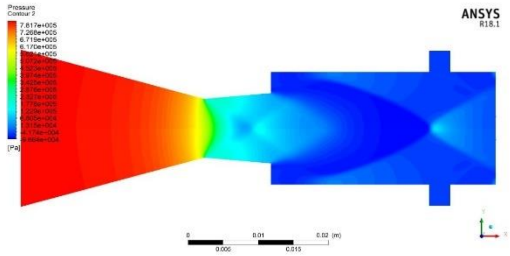

f) NPR 9

Figure 25. The contour results for the model with L/D 2, cavity ASR 1, and cavity location 1.5D.

Table 15. The model geometry for Group 3 with L/D 3.

Group	**3**
L/D	3
Duct length	48 mm
Cavity location from the base wall	1.5D (22.5mm)
Cavity aspect ratio	1

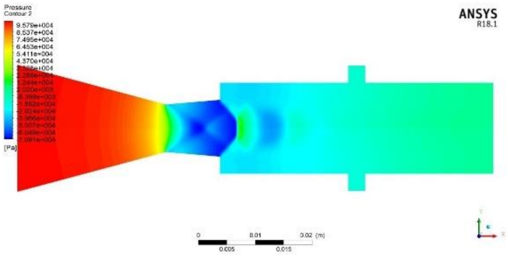

a) NPR 2

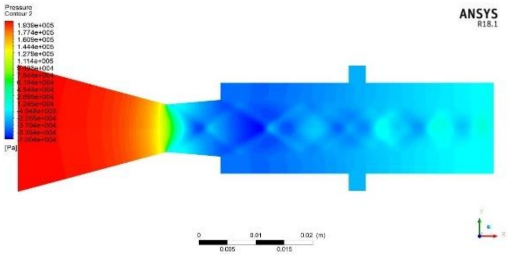

b) NPR 3

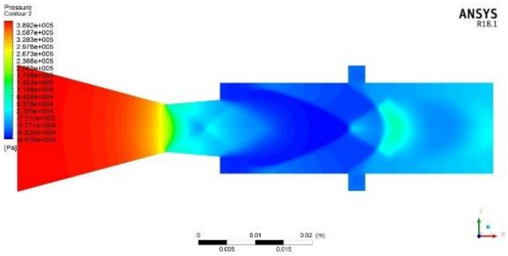

c) NPR 5

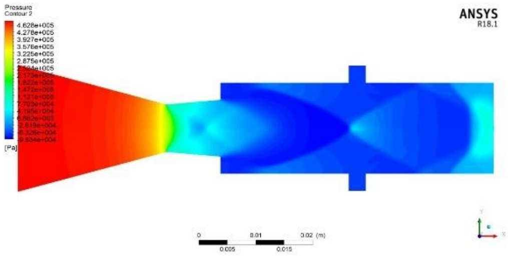

d) NPR 5.75

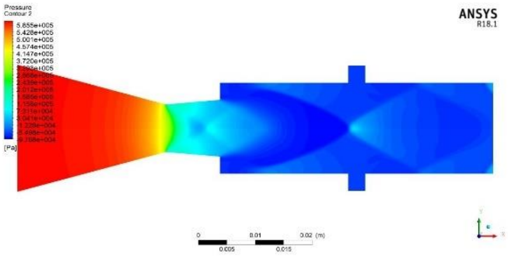

e) NPR 7

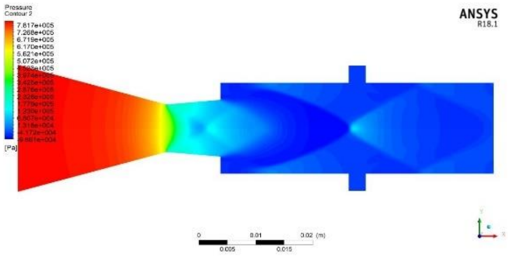

f) NPR 9

Figure 26. The contour results for the model with L/D 3, cavity ASR 1, and cavity location 1.5D.

Table 16. The model geometry for Group 3 with L/D 4.

Group	3
L/D	4
Duct length	64 mm
Cavity location from the base wall	1.5D (22.5mm)
Cavity aspect ratio	1

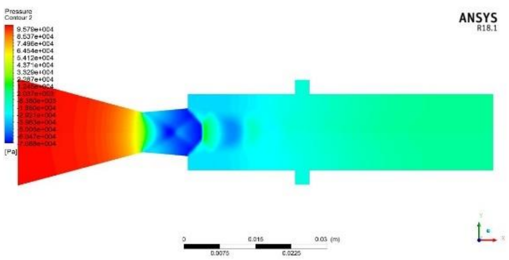

a) NPR 2

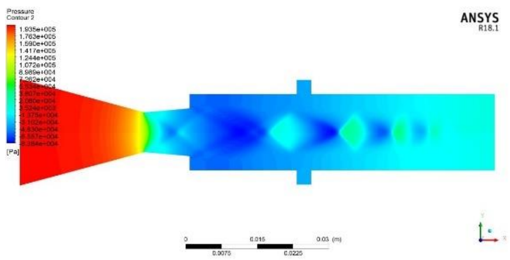

b) NPR 3

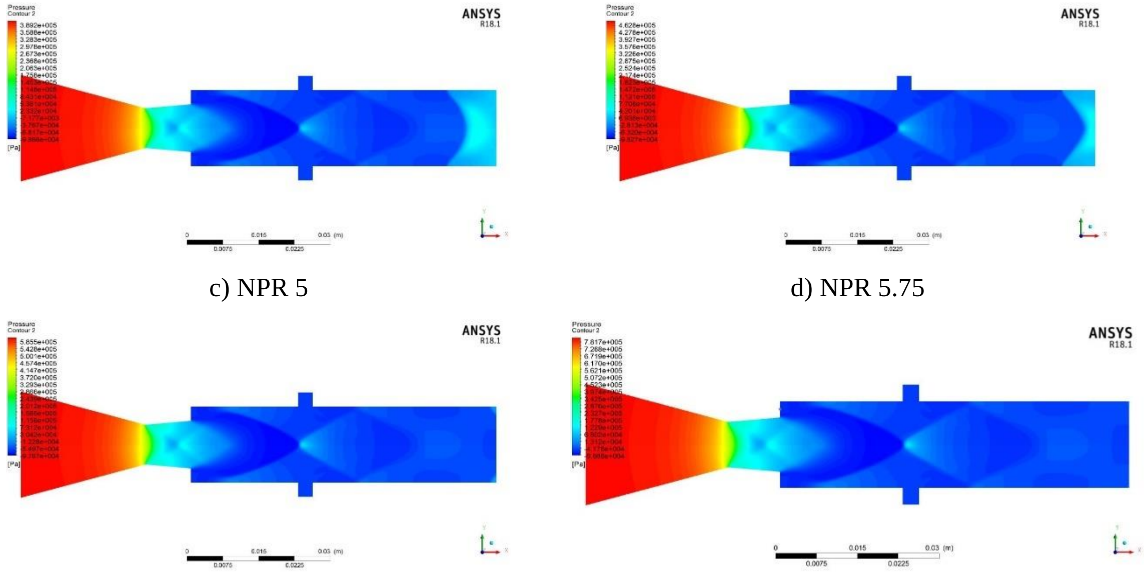

c) NPR 5 d) NPR 5.75

e) NPR 7 f) NPR 9

Figure 27. The contour results for the model with L/D 4, cavity ASR 1, and cavity location 1.5D.

CONCLUSION

In conclusion, in this study, the passive control effectiveness in the form of the cavity to regulate the base pressure is demonstrated. At Mach number 1.8 and area ratio 2.56, a cavity in the duct influenced the base pressure. The pressure contours at various NPR and L/D are studied and illustrated in detail, which will be extremely useful for understanding the pressure variations in the nozzle and duct. Compared to a plain duct, the presence of a cavity at the duct significantly impacts the base pressure. The greater the distance between the cavity location and the base, the greater the base pressure. The pressure gradient based on contour results shows that the passive control has no adverse effect on the wall pressure.

REFERENCES

[1] D.P. Raymer,“Aircraft Design: A Conceptual Approach (Aiaa Education) (AIAA Education Series) (6th ed.) [E-book]“, American Institute of Aeronautics & Ast, 2018.

[2] R.S. WICK, „The Effect of Boundary Layer on Sonic Flow Through an Abrupt Cross-Sectional Area Change“ Journal of the Aeronautical Sciences, Vol. 20, No. 10, Pp. 675–682, 1953. https://doi.org/10.2514/8.2794

[3] K. Pandey, E. Rathakrishnan, “Annular Cavities for Base Flow Control”, *International Journal of Turbo and Jet Engines*, Vol. 23, No. 2, 2006. https://doi.org/10.1515/tjj.2006.23.2.113

[4] W. Nusselt, "Heat Dissipation From Horizontal Tubes and Wires to Gases and Liquids." Ver DeutIng, Vol. 73, Pp. 1475- 1478, 1929.

[5] H. Korst, “A theory of base pressure in transonic and supersonic flow,“ J. Applied Mechanics, Vol. 23, No. 4, 593-600, 1956.

[6] J.S. Anderson, and T. J. Williams, "Base pressure and noise produced by the abrupt expansion of air in a cylindrical duct." Journal of Mechanical Engineering Science, Vol. 10, No. 3, Pp. 262-268, 1968. https://doi.org/10.1243/JMES_JOUR_1968_010_038_02

[7] R. Srikanth, and E. Rathakrishnan, "Flow-through pipes with sudden enlargement," Mechanics Research Communications, Vol. 18, No. 4, 199-206, 1991. https://doi.org/10.1016/0093-6413(91)90067-7

[8] M. Asadullah, S.A. Khan, M.E.M. Soudagar, and T.R. Vaishak, “A comparison of the Effect of Single and Multiple Cavities on Base Flows,” 2018 IEEE 5th International Conference on Engineering Technologies & Applied Sciences, 2019.

[9] M. Asadullah, S.A. Khan, W. Asrar, and E. Sulaeman, “Passive control of base pressure with static cylinder at supersonic flow,” Int. Conf. Aerosp. Mech. Eng., vol. 370, Pp. 012050, 2018, doi: 10.1088/1757-899X/370/1/012050.

[10] S.A. Khan and M. Asadullah, “Grooved Cavity as a Passive Controller behind Backward Facing Step,” J. Adv. Res. Fluid Mech. Therm. Sci., Vol. 53, No. 2, Pp. 185–193, 2019.

[11] M. Asadullah and S.A. Khan, “A Comparison of the Effect of Single and Multiple Cavities on Base Flows,” 2018 IEEE 5th Int. Conf. Eng. Technol. Appl. Sci., no. February, Pp. 1–6, 2019.

[12] S.A. Khan, M. Asadullah, and J. Sadhiq, “Passive Control of Base Drag Employing Dimple in Subsonic Suddenly Expanded Flow,” Int. J. Mech. Mechatronics Eng. IJMME-IJENS, Vol. 18, Pp. 3, 2018.

[13] S.A. Khan and M. Asadullah, “Passive Control of Base Drag in Compressible Subsonic Flow using Multiple Cavity,” Int. J. Mech. Prod. Eng. Res. Dev., vol. 8, no. 4, Pp. 39–44, 2018, doi: 10.24247/ijmperdaug20185.

[14] M. Tanner, “The base cavity at angles of incidence“, AIAA Journal, Vol. 26, No. 3, Pp. 376–377, 1988. https://doi.org/10.2514/3.9903

[15] P.R. Viswanath, and S.R. Patil, “Effectiveness of passive devices for axisymmetric base drag reduction at Mach 2“, Journal of Spacecraft and Rockets, Vol. 27, No. 3, Pp. 234–237, 1990. https://doi.org/10.2514/3.26130

[16] P.R. Viswanath, “Flow management techniques for base and afterbody drag reduction“, Vol. 32, No. 2-3, Pp. 79–129, 1996. doi:10.1016/0376-0421(95)00003-8.

[17] W.A. Mair, “The effect of a rear-mounted disc on the drag of a blunt-based body of revolution“, Aero. Quarterly, Vol. 16, Pp. 350-360, 1965.

[18] E. Rathakrishnan, “Effect of Splitter Plate on Bluff Body Drag“, AIAA Journal, Vol. 37, No. 9, Pp. 1125–1126, 1999. https://doi.org/10.2514/2.823

[19] E. Rathakrishnan, “Effect of Ribs on Suddenly Expanded Flows“, AIAA Journal, Vol. 39, No. 7, Pp. 1402–1404, 2001. https://doi.org/10.2514/2.1461

[20] R. Koomullil, B. Soni, and R. Singh, “A comprehensive generalized mesh system for CFD applications“, Mathematics and Computers in Simulation, Vol. 78, No. 5–6, Pp. 605–617, 2008a. https://doi.org/10.1016/j.matcom.2008.04.005

[21] S.A. Khan, M. Asadullah, F.A.G.M., A. Jalaluddeen, and M.A. Ali Baig, “Flow control with aerospike behind bluff body,” Int. J. Mech. Prod. Eng. Res. Dev., Vol. 8, No. 3, Pp. 1001–1008, 2018, doi: 10.24247/ijmperdjun2018106.

[22] M.H. Azami, M. Faheem, A. Aabid, I. Mokashi, and S.A. Khan, “Inspection of Supersonic Flows in a CD Nozzle using Experimental Method,” Int. J. Recent Technol. Eng., Vol. 8, No. 2S3, Pp. 996–999, 2019.

[23] A. Aabid, F.A.G.M, and Sher Afghan K, “Experimental Investigation of Wall Pressure Distribution in a Suddenly Expanded Duct from a Convergent-Divergent Nozzle,” in 2019 6th IEEE International Conference on Engineering Technologies and Applied Sciences (ICETAS), Pp. 6, 2019. doi: 10.1109/ICETAS48360.2019.9117428.

[24] A. Aabid and S.A. Khan, “Determination of wall pressure flows at supersonic Mach numbers,” Mater. Today Proc., vol. 38, Pp. 2347–2352, 2021, doi: 10.1016/j.matpr.2020.06.538.

[25] A. Aabid, S.A. Khan, and M. Baig, “A Critical Review of Supersonic Flow Control for High-Speed Applications,” Appl. Sci., Vol. 11, No. 15, Pp. 6899, 2021.

[26] A. Aabid, S.A. Khan, M. Ahmed, A. Baig, and K.S. Rao, “Effect of Control on the Duct Flow at High Mach Numbers,” IOP conf. Ser. Mater. Sci. Eng., Vol. 1057, No. 012053, Pp. 9, 2021, doi: 10.1088/1757-899X/1057/1/012053.

[27] A. Aabid, S.A. Khan, M. Ahmed, A. Baig, and A.R. Reddy, “Investigation of Flow Growth in a Duct Flows for Higher Area Ratio,” IOP conf. Ser. Mater. Sci. Eng., Vol. 1057, No. 012052, Pp. 10, 2021, doi: 10.1088/1757-899X/1057/1/012052.

[28] A. Aabid and S.A. Khan, “Studies on Flows Development in a Suddenly Expanded Circular Duct at Supersonic Mach Numbers,” Int. J. Heat Technol., Vol. 39, No. 1, Pp. 185–194, 2021.

[29] F.A.G.M.M. Asadullah, and S.A. Khan, “Experimental Study of Suddenly Expanded Flow From Correctly Expanded Nozzles,” ARPN J. Eng. Appl. Sci., Vol. 11, No. 16, Pp. 10041–10047, 2016.

[30] S.A. Khan, Z. Ahmed, A. Aabid, and I. Mokashi, “Experimental research on flow development and control effectiveness in the duct at high speed,” Int. J. Recent Technol. Eng., Vol. 8, No. 2 Special Issue 8, Pp. 1763–1768, Aug. 2019, doi: 10.35940/ijrte.B1149.0882S819.

[31] S.A. Khan, A. Aabid, and Z.I. Chaudhary, “Influence of control mechanism on the flow field of duct at mach 1.2 for area ratio 2.56,” Int. J. Innov. Technol. Explor. Eng., vol. 8, no. 6 Special Issue 4, Pp. 1135–1138, 2019, doi: 10.35940/ijitee.F1236.0486S419.

[32] M.N. Akhtar, E.A. Bakar, A. Aabid, and S.A. Khan, “Effects of micro jets on the flow field of the duct with sudden expansion,” Int. J. Innov. Technol. Explor. Eng., Vol. 8, No. 9 Special Issue 2, Pp. 636–640, 2019, doi: 10.35940/ijitee.I1129.0789S219.

[33] M.N. Akhtar, E.A. Bakar, A. Aabid, and S.A. Khan, “Control of CD nozzle flow using microjets at mach 2.1,” Int. J. Innov. Technol. Explor. Eng., Vol. 8, No. 9 Special Issue 2, Pp. 631–635, Jul. 2019, doi: 10.35940/ijitee.I1128.0789S219.

[34] S.A. Khan, A. Aabid, I. Mokashi, and Z. Ahmed, “Effect of Micro Jet Control on the Flow Filed of the Duct at Mach 1.5,” Int. J. Recent Technol. Eng., Vol. 8, No. 2S8, Pp. 1758–1762, 2019, doi: 10.35940/ijrte.B1148.0882S819.

[35] S.A. Khan, I. Mokashi, A. Aabid, and M. Faheem, “Experimental Research on Wall Pressure Distribution in C-D Nozzle at Mach number 1.1 for Area Ratio 3.24,” Int. J. Recent Technol. Eng., Vol. 8, No. 2S3, Pp. 971–975, 2019, doi: 10.35940/ijrte.B1182.0782S319.

[36] S.A. Khan, A. Aabid, and C.A. Saleel, “Influence of Micro Jets on the Flow Development in the Enlarged Duct at Supersonic Mach number,” Int. J. Mech. Mechatronics Eng. IJMME-IJENS, Vol. 19, No. 01, Pp. 70–82, 2019.

[37] M. Faheem, M. Kareemullah, A. Aabid, I. Mokashi, and S.A. Khan, “Experiment on of nozzle flow with sudden expansion at mach 1.1,” Int. J. Recent Technol. Eng., Vol. 8, No. 2 Special Issue 8, Pp. 1769–1775, Aug. 2019, doi: 10.35940/ijrte.B1150.0882S819.

[38] M.H. Azami, M. Faheem, A. Aabid, I. Mokashi, and S.A. Khan, “Experimental research of wall pressure distribution and effect of micro jet at Mach 1.5,” Int. J. Recent Technol. Eng., Vol. 8, No. 2 Special Issue 3, 2019, doi: 10.35940/ijrte.B1187.0782S319.

[39] S.A. Khan, A. Aabid, and A.S.C., “CFD Simulation with Analytical and Theoretical Validation of Different Flow Parameters for the Wedge at Supersonic Mach Number,” Int. J. Mech. Mechatronics Eng., vol. 19, no. 1, Pp. 170–177, 2019.

[40] M.N. Akhtar, E.A. Bakar, A. Aabid, and S.A. Khan, “Numerical Simulations of a CD Nozzle and the Influence of the Duct Length,” Int. J. Innov. Technol. Explor. Eng., vol. 8, no. 9S2, pp. 622–630, 2019.

[41] S. A. Khan, A. Aabid, F. A. G. M, A. A. Al-Robaian, and A. S. Alsagri, “Analysis of Area Ratio In a CD Nozzle with Suddenly Expanded Duct using CFD Method,” CFD Lett., vol. 11, no. 5, pp. 61–71, 2019.

[42] A. Aabid, Z. I. Chaudhary, and S. A. Khan, “Modelling and Analysis of Convergent Divergent Nozzle with Sudden Expansion Duct using Finite Element Method,” J. Adv. Res. Fluid Mech. Therm. Sci. J. homepage, vol. 63, no. 1, pp. 34–51, 2019, [Online]. Available: www.akademiabaru.com/arfmts.html.

[43] A. G. M. Fharukh, A. A. Alrobaian, A. Aabid, and S. A. Khan, "Numerical Analysis of Convergent-Divergent Nozzle Using Finite Element Method," Int. J. Mech. Prod. Eng. Dev., vol. 8, no. 6, pp. 373–382, 2018, [Online]. Available: www.tjprc.org.

[44] A. Khan, A. Aabid, and S. A. Khan, "CFD analysis of convergent-divergent nozzle flow and base pressure control using micro-JETS," Int. J. Eng. Technol., vol. 7, no. 3.29, 2018.

[45] S. A. Khan and A. Aabid, "CFD Analysis of CD Nozzle and Effect of Nozzle Pressure Ratio on Pressure and Velocity For Suddenly Expanded Flows," Int. J. Mech. Prod. Eng. Res. Dev., vol. 8, no. June, pp. 1147–1158, 2018.

[46] A. Aabid, A. Khan, N. M. Mazlan, M. A. Ismail, M. N. Akhtar, and S. A. Khan, "Numerical Simulation of Suddenly Expanded Flow at Mach 2.2," Int. J. Eng. Adv. Technol., vol. 8, no. 3, pp. 457–452, 2019.

[47] S. A. Khan, A. Aabid, I. Mokashi, A. A. Al-Robaian, and A. S. Alsagri, "Optimization of two-dimensional wedge flow field at supersonic mach number," CFD Lett., 2019, [Online]. Available: http://www.scopus.com/inward/record.url?eid=2-s2.0-85068619616&partnerID=MN8TOARS.

[48] A. Khan, N. M. Mazlan, and M. A. Ismail, "Analysis of flow through a convergent nozzle at Sonic Mach Number for Area Ratio 4," J. Adv. Res. Fluid Mech. Therm. Sci., vol. 62, no. 1, pp. 66–79, 2019.

[49] A. Khan, N. M. Mazlan, M. A. Ismail, and M. N. Akhtar, "Experimental and numerical simulations at sonic and supersonic mach numbers for area ratio 7.84," CFD Lett., vol. 11, no. 5, pp. 50–60, 2019.

[50] K. A. Pathan, P. S. Dabeer, and S. A. Khan, "Investigation of base pressure variations in internal and external suddenly expanded flows using CFD analysis," CFD Lett., vol. 11, no. 4, pp. 32–40, 2019.

[51] K. A. Pathan, S. A. Khan, and P. S. Dabeer, "CFD analysis of effect of area ratio on suddenly expanded flows," 2nd Int. Conf. Converg. Technol. I2CT 2017, vol. 2017-Janua, pp. 1192–1198, 2017, doi: 10.1109/I2CT.2017.8226315.

[52] K. A. Pathan, P. S. Dabeer, and S. A. Khan, "Influence of expansion level on base pressure and reattachment length," CFD Lett., vol. 11, no. 5, pp. 22–36, 2019.

[53] K. A. Pathan, P. S. Dabeer, and S. A. Khan, "Enlarge duct length optimization for suddenly expanded flows," Adv. Aircr. Spacecr. Sci., vol. 7, no. 3, pp. 203–214, 2020.

[54] A. Aabid and S. A. Khan, "Investigation of High-Speed Flow Control from CD Nozzle Using Design of Experiments and CFD Methods," Arab. J. Sci. Eng., vol. 46, no. 3, pp. 2201–2230, 2021, doi: 10.1007/s13369-020-05042-z.

[55] J. D. Quadros, S. A. Khan, and T. Prashanth, "Experimental and numerical investigation of expansion corner effects on isolator performance," Int. J. Tu, 2020.

[56] L. Kharulaman, A. Aabid, F. Ahmed, G. Mehaboobali, and S. A. Khan, "Research on Flows for NACA 2412 Airfoil using Computational Fluid Dynamics Method," Int. J. Eng. Adv. Technol., vol. 9, no. 1, pp. 5450–5456, 2019, doi: 10.35940/ijeat.A3085.109119.

[57] A. Aabid, L. Nabilah, B. Khairulaman, and S. A. Khan, "Analysis of Flows and Prediction of CH10 Airfoil for Unmanned Arial Vehicle Wing Design," Adv. Aircr. Spacecr. Sci., vol. 8, no. 2, p. 24, 2021, doi: https://doi.org/10.12989/aas.2021.8.2.087.

[58] S. A. Khan, A. Aabid, I. Mokashi, A. A. Al-Robaian, and A. S. Alsagri, "Optimization of Two-dimensional Wedge Flow Field at Supersonic Mach Number," CFD Lett., vol. 11, pp. 80–97, 2019.

[59] S. A. Khan, A. Aabid, and A. S. C., "CFD Simulation with Analytical and Theoretical Validation of Different Flow Parameters for the Wedge at Supersonic Mach Number," *Int. J. Mech. Mechatronics Eng.*, vol. 19, no. 1, pp. 170–177, 2019.

[60] M. F. M. Sajali, S. Ashfaq, A. Aabid, and S. A. Khan, "Simulation of Effect of Various Distances between Front and Rear Body on Drag of a Non-Circular Cylinder," J. Adv. Res. Fluid Mech. Therm. Sci., vol. 62, no. 1, pp. 53–65, 2019.

[61] M. F. M. Sajali, A. Aabid, S. A. Khan, F. A. G. Mehaboobali, and E. Sulaeman, "Numerical investigation of flow field of a non-circular cylinder," CFD Lett., vol. 11, no. 5, pp. 37–49, 2019.

[62] A. Afifi, A. Aabid, and S. Afghan Khan, "Numerical investigation of splitter plate effect on bluff body using finite volume method," Mater. Today Proc., vol. 38, pp. 2181–2190, 2021, doi: 10.1016/j.matpr.2020.05.559.

[63] A. Aabid, A. Afifi, F. Ahmed Ghasi Mehaboob Ali, M. Nishat Akhtar, and S. Afghan Khan, "CFD Analysis of Splitter Plate on Bluff Body," CFD Lett., vol. 11, pp. 25–38, 2019.

[64] A. Afzal, S. A. Khan, M. T. Islam, R. D. Jilte, A. Khan, and M. E. M. Soudagar, "Investigation and back-propagation modeling of base pressure at sonic and supersonic Mach numbers," Phys. Fluids, vol. 32, no. 9, 2020, doi: 10.1063/5.0022015.

[65] A. Afzal, A. Aabid, A. Khan, S. A. Khan, T. Nath, and R. Kumar, "Response surface analysis, clustering, and random Forest regression of pressure in suddenly expanded high-speed aerodynamic flows," Aerosp. Sci. Technol., vol. 1, p. 106318, 2020, doi: 10.1016/j.ast.2020.106318.

[66] J.D. Quadros, S.A. Khan, S. Sapkota, J. Vikram, and T. Prashanth, "On Recirculation Region Length of Suddenly Expanded Supersonic Flows, Using CFD and Fuzzy Logic," Int. J. Comut. Fluid Dyn., vol. 0, no. 0, pp. 1–16, 2020, doi: 10.1080/10618562.2020.1828580.

[67] R. Koomullil, B. Soni, and R. Singh, 2008b. A comprehensive generalized mesh system for CFD applications. Mathematics and Computers in Simulation, 78 (5–6), Pp. 605–617. https://doi.org/10.1016/j.matcom.2008.04.005